Communications Research Centre

SYSTEM-DESIGN CONSIDERATIONS FOR AN OPTICAL CORRELATOR FOR THE SEASAT-A SYNTHETIC-APERTURE RADAR

by

E.B. Felstead

This work was sponsored by the Department of National Defence, Research and Development Branch, under Project No. 33D16

DEPARTMENT OF COMMUNICATIONS
MINISTÈRE DES COMMUNICATIONS

CRC REPORT NO. 1321

CANADA

OTTAWA, APRIL 1979

COMMUNICATIONS RESEARCH CENTRE

DEPARTMENT OF COMMUNICATIONS
CANADA

SYSTEM-DESIGN CONSIDERATIONS FOR AN OPTICAL CORRELATOR FOR THE SEASAT-A SYNTHETIC-APERTURE RADAR

by

E.B. Felstead

(Radio and Radar Research Branch)

CRC REPORT NO. 1321

APRIL 1979
OTTAWA

This work was sponsored by the Department of National Defence, Research and Development Branch, under Project No. 33D16

TABLE OF CONTENTS

SYSTEM-DESIGN CONSIDERATIONS FOR AN OPTICAL CORRELATOR FOR THE SEASAT-A SYNTHETIC-APERTURE RADAR

by

E.B. Felstead

ABSTRACT

System-design considerations are presented for an optical correlator that processes signals recorded on film from the synthetic-aperture radar of the SEASAT-A satellite. A strip-map image of the earth's surface is to be produced with a resolution down to 6.5 m along track (azimuth) and 25 m across track (range). The input film and the two-dimensional Fourier transform are described mathematically and their parameters given. Processing problems introduced by range curvature, antenna pitch and yaw, earth rotation, low PRF, etc. are handled by simple modifications to a standard tilted-plane correlator. Recommended system configurations, output parameters and system limitations are given.

1. INTRODUCTION

One of the instruments on board the SEASAT-A remote-sensing satellite is a synthetic-aperture radar (SAR) operating at L-band. Data from this SAR is to be recorded optically on film, in the form of interferograms. These interferograms are then to be processed by an optical correlator to produce images of the earth's surface in the form of strip maps.

As part of the Canadian effort for the SEASAT-A experimental program, the Department of National Defence through the Defence Research Establishment Ottawa (DREO) has undertaken the task of designing and building a suitable optical correlator. This correlator is to be capable of producing imagery from interferograms obtained from an optical recorder to be installed at the Shoe Cove, Newfoundland receiving station. The correlator itself will be installed in a laboratory at DREO.

DREO has also undertaken the task of providing the recorder. Design considerations and characteristics of the output of this recorder are given in [1] and in numerous subsequent unpublished memoranda; many of the symbols used in [1] will be used here without redefinition. The operation of the recorder and correlator are highly interdependent. Thus, to a certain extent, both must be designed simultaneously. The design procedure is, in fact, iterative: if one device is altered, the other must be altered to match. Furthermore, the design of the recorder is influenced by the desire to make interferograms with the same format as those to be produced by Jet Propulsion Laboratories (JPL). With such compatibility it should be possible for JPL to process DREO interferograms, and vice versa.

The purpose of this report is to present a preliminary specification and system design for the correlator system. The detailed component design will be the responsibility of the contractor. The general theory of satellite-borne SAR given in [2] is used as the basis for this system design.

2. TILTED-PLANE VERSUS TILTED-LENS CORRELATORS

When plane-wave monochromatic light passes through a SAR interferogram, an erect range-image and a tilted azimuth-image are produced. The object of the correlator is to produce a two-dimensional output image wherein the two image-planes are exactly superimposed or coplanar. The "tilted-plane method", developed at the University of Michigan Willow Run Laboratories (now the Environmental Research Institute of Michigan or ERIM), uses sets of telescopic imagers to effect the superposition [3]. The "tilted-lens method" developed and extensively used by Goodyear Aerospace uses a tilted cylindrical lens to de-tilt the azimuth image.

In the tilted-lens method, the tilted lens introduces aberrations that do not occur in the tilted-plane method. These aberrations are the main disadvantage of the tilted-lens method. A second disadvantage is that it is more difficult to incorporate a variable-aspect-ratio facility in a tilted-lens processor.

The tilted-plane correlator also has disadvantages. First, it is usually of greater length than a tilted-lens correlator, but this is not a problem for the proposed new correlator. Second, the amount of erection is proportional to the square $(1/A_o)^2 = K_o^2$ of the aspect ratio of the optical correlator. Therefore K_o should be as large as possible and cannot be ≤ 1 or no erection will occur. However, as discussed in the previous report on the recorder [1], with SEASAT-A an ingenious technique is possible, wherein the production of a unity-aspect-ratio, erect image is combined with the conversion of slant-range coordinates to ground-range coordinates. With this technique, the tilted-plane processor seems quite satisfactory for SEASAT-A processing.

For the above reasons, and since all the experience with correlators at DREO has been with the tilted-plane design, it is recommended that the tilted-plane processor be utilized. Note that JPL is also using a tilted-plane processor.

3. DESCRIPTION OF DATA AND RELEVANT SEASAT CHARACTERISTICS

3.1 MATHEMATICAL DESCRIPTION OF THE INTERFEROGRAM DATA

The mathematical description of the interferogram data is taken from [2]. This description is based on a natural coordinate system, wherein the azimuth coordinate is taken along the projection of the actual satellite flight-path along the surface of the earth. For a point object located in the natural coordinate system at azimuth and slant range (x_o, r_o), respectively, the recorded data will have the form

$$g(x_f,r_f) = b\sigma \sum\delta(x_f - nv_f/f_p)\; h\left[\frac{x_f - \dfrac{x_o - x_{py}(r_o) - x_{ye}(r_o)}{p}}{r_o\beta/p}\right]$$

$$f\left\{\frac{2q}{c}\left[r_f - \frac{r_o}{q} - \frac{c_a p^2}{2qr_o}(x_f - x_o/p)^2\right]\right\}$$

$$\exp(j2\pi f_{or} r_f)\exp -j\,\frac{4\pi}{\lambda_r}\left[r_o + \frac{c_a p^2}{2r_o}(x_f - x_o/p)^2\right]$$

$$+ \text{c.c.} + B \qquad (3.1)$$

(x_f, r_f) = azimuth and range coordinates on film

$f_{or} = f_o/v_c$ = spatial frequency offset in range

v_c = velocity of recording beam across film - see [1]

v_f = velocity of film during recording - see [1]

f_p = pulse repetition frequency (PRF) in Hz

h = two-way antenna pattern in azimuth

β = two-way angular beamwidth of antenna

$c_a = 1 + h_s/r_e$ = constant relating velocity of satellite to velocity of projection on surface

$p = (V/c_a)/v_f$ = azimuth demagnification

$q = c/(2v_c)$ = range demagnification

V = velocity of satellite relative to stationary earth

h_s = altitude of satellite

x_{py} = azimuth offset of centre of antenna beam due to pitch and yaw

x_{ye} = azimuth offset of centre of antenna beam due to equivalent yaw [2]

$r_o\beta/p$ = azimuth aperture

λ_r = wavelength of radar

$f[2q/c\ (r_f - r/q)]$ = range signal

$$= \text{rect}\left[\frac{r_f - r/q}{R_2/2q}\right] e^{j\pi s(2q/c)^2(r_f - r/q)^2} \tag{3.2}$$

$$r = r_o + \frac{c_a p^2}{2r_o}(x_f - x_o/p)^2 \tag{3.3}$$

B_2 = bandwidth of range pulse

$R_2 = cT_r$ = pulse length in space

T_r = pulsewidth in time

s = sweep rate of range linear FM in Hz/s

$R_2/2q$ = width of range pulse on film

c.c. = complex conjugate of the previous term

B = bias level, chosen to place operation in centre of linear region of the film's amplitude transmittance versus exposure curve

b = scaling factor, chosen to keep signal within linear region of the film's amplitude transmittance versus exposure curve

σ = radar reflectivity of target

The offsets of the antenna pattern h arising from pitch, yaw, and equivalent yaw are range dependent and are given by [2]

$$x_{py} = h_s\,\theta_p - \sqrt{r_o^2 - h_s^2}\,\theta_y \tag{3.4}$$

and

$$x_{ye} = \sqrt{r_o^2 - h_s^2}\ \frac{V_{en}}{V_{sp}/c_a} \tag{3.5}$$

where

θ_p = pitch angle of antenna

θ_y = yaw angle of antenna

$V_{en} = \omega_e r_e \sin\theta_i \cos\phi_o$ = velocity of earth normal to $\underline{V}_s$

$V_{ep} = \omega_e r_o \cos\theta_i$ = velocity of earth parallel to $\underline{V}_s$

$V_{sp} = V_s - c_a V_{ep}$ = component of $\underline{V}$ parallel to $\underline{V}_s$

V_s = velocity of satellite in inertial space

$$V = \sqrt{(c_a V_{en})^2 + (V_s - c_a V_{ep})^2}$$

θ_i = orbital inclination

ϕ_o = angular distance along orbit; $\phi_o = 0$ at equator.

It was pointed out to the author by T.J. Bicknell of JPL that SEASAT-A will have a vertical velocity component V_v, and that the major effect is equivalent to an additional pitch of the antenna. The equivalent pitch angle is $\theta_v = \tan^{-1}(V_v/V)$ so that the additional offset of antenna pattern h is

$$x_v = h_s \tan^{-1}(V_v/V).$$

This value is added to $x_{py}+x_{ye}$ to obtain the total effective pitch and yaw offset.

If h is a rect function then the Rayleigh resolution in azimuth is

$$\rho_{Ra} = \lambda_r/(2c_a\beta)$$

and the -3-dB resolution is $0.886\ \rho_{Ra}$.

More generally the -3-dB resolution is

$$\rho_{3a} = \mu_a\lambda_r/(2c_a\beta)$$

where μ_a is a constant depending on the form of function h. The Rayleigh slant-range resolution is

$$\rho_{Rrs} = \frac{c}{2B_2}$$

and the ground range resolution is seen from (3.9) to be

$$\rho_g = \frac{c_r}{\sqrt{1 - (h_s/r_{sav})^2}}\,\rho_{rs}$$

where c_r is given in (3.6).

3.2 RELEVANT SEASAT-A PARAMETERS

In this subsection various parameters of the SEASAT-A satellite that will be needed in designing and operating the correlator are given. Basic parameters are given in Table 3.1, and this table is followed by discussions

on parameters related to range and antenna attitude. The values given in this subsection were ones available at the time of writing, and are not guaranteed to be final values. Furthermore, for many of the parameters, conflicting values have been obtained from different sources. Thus, values given here are not necessarily accurate.

TABLE 3.1

Some Parameters of SEASAT-A Relevant to the Correlator

λ_r = 0.235 m

f_o = 11.3824 MHz

f_p = f_o/N where N is an integer
= 1463.8, 1539.8, 1580.9 and 1646.8 Hz

h_s = 795 km at latitudes within view of Shoe Cove

V_s = 7.47 km/s

V = 7.64 km/s at latitudes within view of Shoe Cove

c_a = 1.13

T_r = 33.8 μs

B_2 = 19×10^6 Hz

s = $19 \times 10^6/(33.8 \times 10^{-6}) = 0.56 \times 10^{12}$ Hz/s

β = *

$r_o\beta$ = { 13.6 km 1 look full resolution
3.5 km 4 looks reduced resolution } at r_o = 850 km

* *Various values of β have been noted: e.g., 1° (17 mrad) and 16 mrad (0.92°). Also from a 14 April 1977 JPL design review meeting, a drawing of the azimuth antenna pattern shows the 3 dB 2-way width as 0.8° (14.0 mrad). The value 16 mrad will normally be used in this report.*

The angle between the nadir and the antenna boresight, or direction of maximum antenna gain, is nominally 20°, as shown in Figure 3.1. The slant range r_{so} along the boresight may then be calculated to be 853.14 km. The ground range r_g may be calculated from slant range r_s by solving for r_g in

$$r_s = \left\{(h_s+r_e)^2 + r_e^2 - 2r_e(h_s+r_e)\cos(r_g/r_e)\right\}^{\frac{1}{2}} \qquad (3.6)$$

where r_e = radius of the earth = 6371 km. A convenient approximation,

$$r_g \simeq c_r \sqrt{r_s^2 - h_s^2}\ , \qquad (3.7)$$

is obtained from (3.6) by use of the small angle approximation for $\cos(r_g/r_e)$. Here $c_r = 1\sqrt{1 + h_g/r_e} = 0.943$. Thus the boresight ground range r_{go} is 291.90 km.

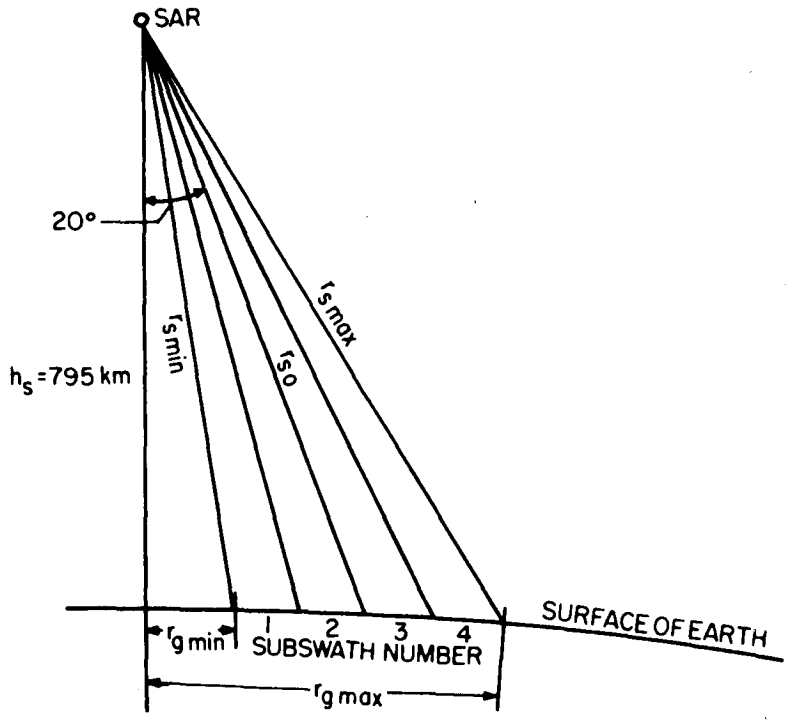

Figure 3.1. Slant, Ground Range and Subswaths

It is desired to use a 100 km swath. If 50 km of ground range are taken on each side of boresight, then the limiting ranges are

$$r_{g\ min} = 241.90 \text{ km}$$

and

$$r_{g\ max} = 341.90 \text{ km}.$$

Substitution of these values in (3.6) gives

$$r_{s\ min} = 835.36 \text{ km}$$

and

$$r_{s\ max} = 873.77 \text{ km}$$

so that the slant-range swath width Δr_s is 38.41 km. The strength of signal

returning from targets at a particular range will depend on antenna pattern, satellite roll, and the sensitivity time control (STC). It is proposed at JPL to process the signals in 4 subswaths. If the slant-range swath Δ_{rs} is divided into 4 equal parts, then the limiting slant ranges for each subswath are as given in Table 3.2. The DREO correlator will not necessarily process these exact subswaths, depending upon various circumstances (see Subsection 3.3). Note that r_{sav} is the average of the maximum and minimum slant range, but r_{gav} as calculated from the nonlinear equation (3.6) would not give an exact average ground range and is therefore not given in Table 3.2.

TABLE 3.2

Ranges in km for 4 Equal Slant Range Subswaths

	Subswath 1	Subswath 2	Subswath 3	Subswath 4
r_{smax}	844.96	854.56	864.17	873.77
r_{sav}	840.16	849.76	859.36	868.96
r_{smin}	835.36	844.96	854.57	864.17
Δr_s	9.60	9.60	9.60	9.60
r_{gmax}	269.92	295.60	319.46	341.90
r_{gmin}	241.90	269.92	295.60	319.46
Δr_g	28.02	25.68	23.86	22.4

In any final map, it is desirable to have the range dimension in units of ground range. The slant-range-to-ground-range conversion (3.6) or (3.7) in general is nonlinear. However, for small r_g/r_e, the derivative of (3.6) is

$$\frac{dr_g}{dr_s} \simeq \frac{c_r}{\sqrt{1 - (h_s/r_s)^2}} \tag{3.8}$$

and over a limited subswath, the slant-range-to-ground-range conversion is approximately linear. Then Δr_g is given approximately by

$$\Delta r_g = \frac{c_r}{\sqrt{1 - (h_s/r_{sav})^2}} \Delta r_s \tag{3.9}$$

where r_{sav} is the average value of slant range over the limited subswath.

Relation (3.9) is linear and is implemented optically by a simple magnification. The magnification M_{rc} required for slant-range-to-ground-range conversion is $M_{rc} = dr_g/dr_s$. In Table 3.3 are given the values of M_{rc} for the average slant ranges r_{sav} for the 4 subswaths of Figure 3.1 and Table 3.2. Also given are the errors ϵ_{mrc} in M_{rc} at the two edges of the subswath. For the worst-case subswath, the magnification error is +5.3% at one edge and -4.5% at the other edge. Thus, for SEASAT-A, range conversion over one subswath can be performed by a simple magnification if magnification errors of up to ±5% at the edges can be tolerated.

TABLE 3.3

Magnification M_{rc} for r_{sav} and its Error ϵ at the Edge of the Subswath

Subswath Number	r_{sav} km	$M_{rc} = dr_g/dr_s$	ϵ_{mrc}	$\frac{\epsilon_{mrc}}{M_{rc}} \times 100$	ϵ_p km
1	840.16	2.916	+0.155	+5.3%	+0.33
			-0.132	-4.5%	
2	849.76	2.670			
3	859.36	2.483			
			+0.070	+3.0%	+0.15
4	868.96	2.336	-0.063	-2.7%	

The positional error at the edge of the subswath at the maximum range is ϵ_p = true ground range, r_{gmax} - ground range calculated from (3.9)

$$= r_{g\ max} - [r_{gav} + M_{rc}(r_{smax} - r_{sav})].$$

A similar relation exists for the minimum range. Two examples are tabulated in Table 3.3 for r_{gmax}. The worst error occurs for subswath 1, with ϵ_p = +0.33 km, which for a resolution of 0.025 km means a worst-case error of 13 resolution cells.

The objective is to obtain 25 m resolution in both azimuth and ground range. For a full azimuth aperture of 16 mrad, the Rayleigh azimuth resolution is $\rho_{Ra} = 0.235/(2x1.13 \times 16 \times 10^{-3}) = 6.5$ m. For 25 m resolution a beamwidth of only $\lambda_r/(2c_a \times 25) = 4.2$ mrad is needed which corresponds to a synthetic aperture of $4.2 \times 10^{-3} \times 850 = 3.5$ km at $r_o = 850$ km. The slant range resolution is $3 \times 10^8/(2 \times 19 \times 10^6) = 7.9$ m. From $\rho_g = M_{re}\ \rho_{rs}$ and Table 3.3, the ground-range Rayleigh resolution is $7.9 \times 2.67 = 21.1$ m at $r_o = 850$ km.

Values of x_{py} and x_{ye} vary with range and latitude. The following values were used in calculating x_{py} and x_{ye}:

$$\theta_i = 108°$$

$$\theta_p\Big|_{max} = \pm 0.5°$$

$$\theta_y\Big|_{max} = \pm 0.5°$$

$$\phi_{lat} = \begin{Bmatrix} 29° \text{ min} \\ 66° \text{ max} \end{Bmatrix} \text{ for range of Shoe Cove [1]}$$

$$\text{which corresponds to } \phi_o = \begin{cases} 30.6° \text{ min} \\ 52.5° \text{ average (value at Shoe Cove)} \\ 73.8° \text{ max} \end{cases}$$

$$\omega_e r_e = 0.463 \times 10^3 \text{ m/s}$$

$$V_{ep} = -143 \text{ m/s}$$

$$V_{sp} = 7.63 \text{ km/s}$$

With these values, Table 3.4 was calculated using (3.4) and (3.5). The worst case combination of $\theta_p|_{max}$ and $\theta_y|_{max}$ were used. To demonstrate the variation with latitude, x_{py} and x_{ye} were calculated at the extremes of the range of Shoe Cove viewing area, using an average value for r_o of 860 km. To demonstrate the variation with range, x_{py} and x_{ye} were calculated for r_o = 841, 860 and 879 km using an average value of $\phi_o = 52.5°$, which corresponds approximately to the latitude of Shoe Cove.

TABLE 3.4

Selected Values of x_{py} and x_{ye}

	$\phi_o = 30.6°$ $r_o = 860$ km	$\phi_o = 73.8°$ $r_o = 860$ km	$\phi_o = 52.5°$ $r_o = 841$ km	$\phi_o = 52.5°$ $r_o = 860$ km	$\phi_o = 52.5°$ $r_o = 879$ km
x_{py} km	9.8	9.8	9.3	9.8	10.2
x_{ye} km	18.4	6.0	10.9	13.0	14.9
worst case sum of $x_{py}+x_{ye}$	28.2	15.8	20.2	22.8	25.1

If the equation for V given after (3.5) is used along with the previously given values of V_s and V_{ep}, then V = 7.642 km/s at $\phi_o = 30.6°$ and V = 7.631 km/s at $\phi_o = 73.8°$. The change in V is approximately 11 m/s; i.e., 0.1%. The variation in the satellite velocity V_s because of orbital factors has been calculated by M. Royer of the Communications Research Centre (CRC) to be of the order of 15 m/s over the entire orbit. Therefore it seems

reasonable to assume that variations in V_s over the Shoe Cove viewing region would be small compared to the 11 m/s calculated for the change in V. Henceforth, variations in V_s will be neglected.

From [4] it appears that, in the Shoe Cove coverage area, the vertical velocity varies between ±5 m/s. Thus $\theta_v|_{max} = \pm 0.038°$ and $x_v|_{max} = \pm 0.52$ km. This value agrees with the JPL estimate that 1 m/s of vertical velocity gives ≈ 100 m shift. Because x_v is small compared to both x_{py} and x_{ye}, and because its effect is identical to x_{py}, x_v will be absorbed in x_{py} for most of this report.

3.3 PARAMETERS OF THE INTERFEROGRAM

The characteristics of the input interferogram listed in Table 3.5 are a corrected form of values given in [1]. These values are based on having compatibility with the interferograms generated by JPL. It is thereby assumed that during recording of the interferogram, the film velocity is $v_f = 40$ mm/s and the beam velocity across the film is $v_c = 4.90 \times 10^5$ mm/s. It is currently proposed to obtain this value of v_c by using a 4.25 inch CRT trace with a 1.36:1 reduction between the CRT and the film.

TABLE 3.5

Characteristics of Interferogram

Film base	preferably acetate but possibly estar
aspect ratio $A_f = q/p$	1.81
RANGE	
film width	5 inch
number of films	2 – total of 4 subswaths
number of subswaths per film	2 – total of 4 subswaths
maximum signal length on one film (exclusive of annotation)	79.3 mm (3.12 inches)
minimum aperture required for one subswath [1]	97.8×10^{-6}s x $4.90 \times 10^5 = 47.9$ mm
range aperture to be used at JPL	50 mm
scale factor q	306,122
highest spatial frequency	42.9 lp/mm
pulsewidth of single target = $R_2/(2q) = cT_r/2q$	16.6 mm
$f_{or} = f_o/v_c$	23.2 c/mm
spatial bandwidth, $B_r = B_2/v_c$	38.8 c/mm
AZIMUTH	
minimum length of one film for a 10 minute pass	24 m (79 ft.)
scale factor p	169,027
minimum azimuth aperture $r_o\beta/p$ yielding one output azimuth resolution cell	
a) for full 6.5 m resolution	13.6 km/p = 80.5 mm
b) for 25 m resolution (using one of 4 looks)	3.5/p = 20.7 mm
aperture to be used at JPL	100 mm
spot size	0.5 mil (13 μm) (equivalent to a MTF of 50% at 31 lp/mm)
worst offset arising from pitch and yaw for r_o = 860 km, x_{py}/p	58.0mm
worst offset due to equivalent yaw for r_o = 860, x_{ye}/p	108.9 mm
worst offset at r_o = 860 due to combined pitch, yaw, and equivalent yaw	166.9 mm

In Table 3.5 and in all subsequent work it is very important to distinguish between measures of spatial frequency for incoherent illumination and for coherent illumination. The interferogram itself is recorded using incoherent light and spatial frequency is therefore measured either in spot size (mm), or, in modulation transfer function (MTF) as a function of line pairs/mm (lp/mm). When the interferogram is placed in the optical correlator, it is illuminated with coherent light so that MTF and lp/mm become meaningless in the description of the operation of the correlator. What is required for the analysis of the correlator is the coherent transfer function (CTF), which is expressed as a function of cycles/mm (c/mm). The distinction between MTF as a function of lp/mm and CTF as a function of c/mm is important when handling bandpass signals and negative spatial frequencies since negative lp/mm is meaningless. In this report, spatial frequencies given in lp/mm will be assumed to refer to incoherent response, and those given in c/mm, to coherent response. Because of the differences between MTF and CTF, the reader is strongly cautioned not to assume automatically that the correlator will have to handle spatial frequencies as high as those implied by the values of the interferogram MTF given in Table 3.5. As will be seen, beam-tilting, etc., can be utilized to reduce the spatial-frequency requirements.

It was recommended in a CRC memorandum of January 1977 that processing be divided into 5 subswaths. That recommendation was based on worst-case considerations of correcting the range curvature. However, it appears that 4 subswaths are going to be employed both for the JPL correlator and for the DREO correlator.

The recording will be made on two films as illustrated in Figure 3.2. On each film is space for 2 subswaths. The films could be processed in 4 subswaths as illustrated; however, it would be useful to make the liquid-gate film-drive assembly of the correlator sufficiently flexible to process a subswath located at any position across the film. It is, of course, permissible to reduce the range aperture during processing to less than the quarter swath width. This may be useful for such things as reducing range-curvature-correction errors. However, the range aperture cannot be reduced to less than a range-pulse length of $T_r v_c = 16.6$ mm.

3.4 FOCUSSING PARAMETERS OF THE INTERFEROGRAM

From (3.1) and (3.2), the carrier for the interferogram has the form

$$\cos\left[2\pi f_{or} r_f - \frac{4\pi}{\lambda_r}\frac{c_a p^2}{2r_o} x_f^2 + \pi s(2q/c)^2 r_f^2\right] \tag{3.10}$$

where here phase constants and the effects of range curvature have been omitted. The sign of s is taken as positive if the range linear FM is swept upwards, and negative if downwards. The lines of constant phase are hyperbolas when the frequency is swept up as in SEASAT-A. The form of the interferogram for a single target is shown in Figure 3.3. Notice that the spatial frequency increases with r_f.

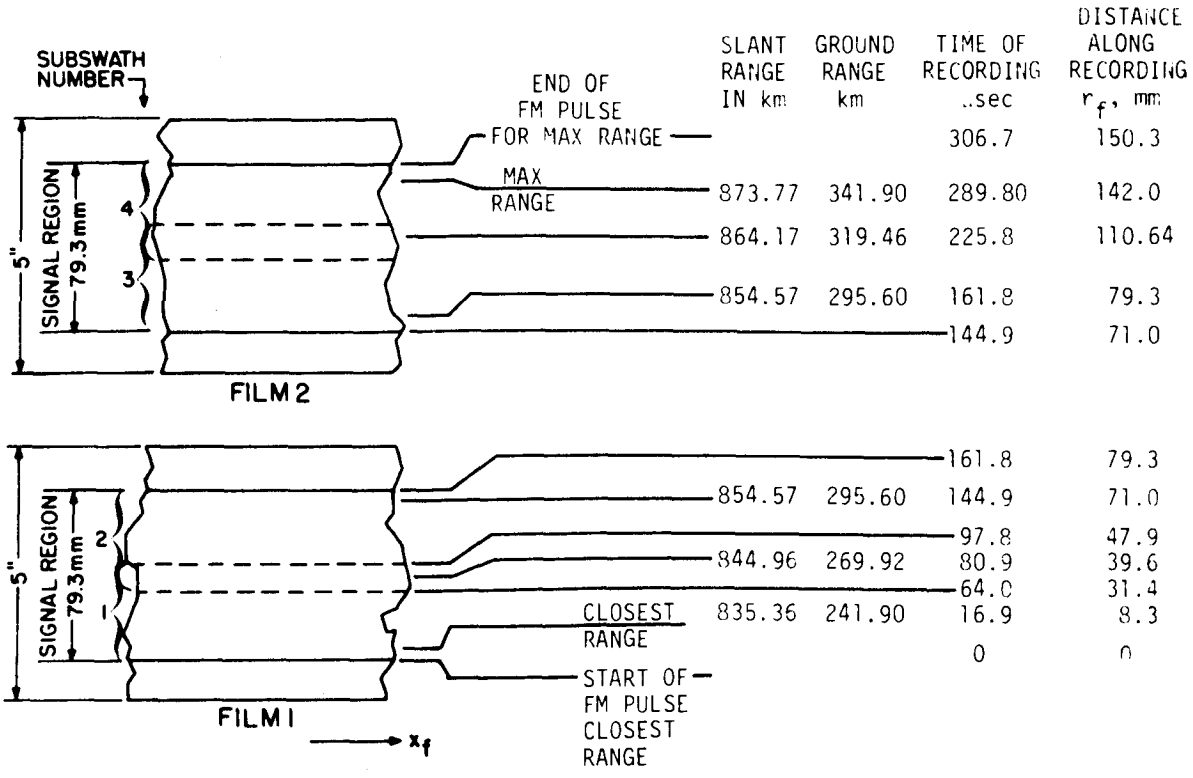

Figure 3.2. Dividing the Film in Range into Subswaths

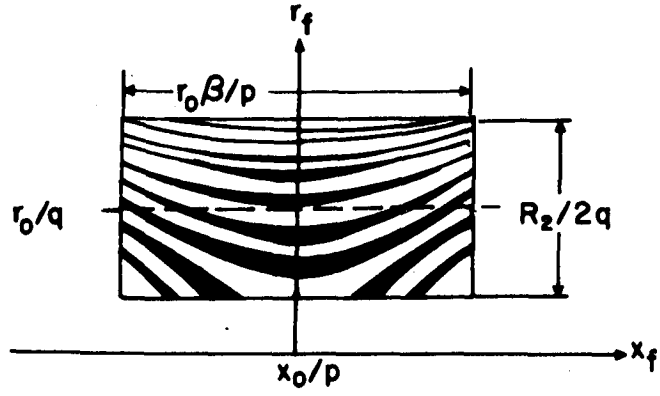

Figure 3.3. Representation of Recording for a Single Object Located at (x_o, r_o)

The amplitude transmittance of a cylindrical lens of focal length F is

$$t_\ell(x) = e^{-j\frac{k}{2F}x^2} \tag{3.11}$$

where $k = 2\pi/\lambda$ and λ is the wavelength of light. By expanding (3.10) into complex exponentials and then comparing with (3.11), it can be seen that the interferogram is the equivalent to 4 cylindrical lenses. For the positive first order in range, there are two equivalent cylindrical "lenses" with focal lengths

$$F_x = + \frac{\lambda_r r_o}{2p^2 \lambda c_a} \tag{3.12}$$

in azimuth and

$$F_r = - \frac{c^2}{4sq^2\lambda} \tag{3.13}$$

in range. When plane-wave monochromatic light is passed through the interferogram, these "lenses" will cause focussing in azimuth to a real image a distance F_x behind the interferogram, and focussing in range to a virtual image a distance F_r in front of the interferogram (if s is positive). A representation of this condition is shown in Figure 3.4. If the negative first order is selected instead, there will be a real range image and a virtual azimuth-image. The rays will be tilted at an angle $\phi_{or} = \sin^{-1}(\lambda f_{or}) \simeq \lambda f_{or}$ to the optical axis, as shown in Figure 3.4, because of the spatial carrier frequency f_{or} in range. Typical focal lengths are given in Table 3.6 for the extreme ranges of the 4 subswaths given in Figure 3.2. The signs are for the positive first order; if the negative first order is used, the signs are to be reversed. A illumination wavelength $\lambda = 0.6328$ μm was assumed in the calculation.

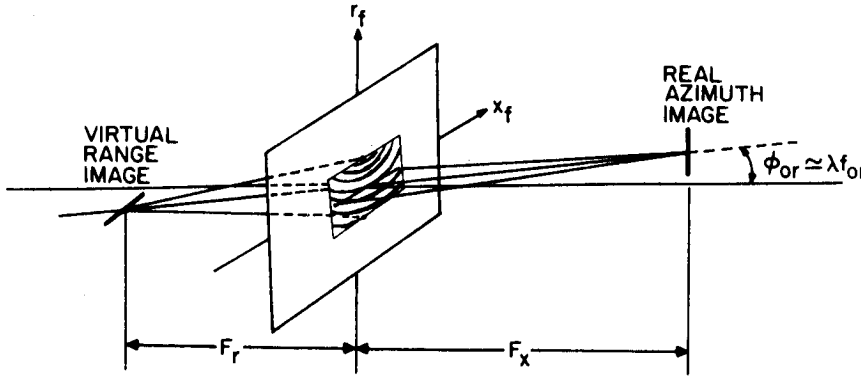

Figure 3.4. Real azimuth image and virtual range image for positive first order. Images are aligned at an angle $\phi_{or} \simeq \lambda f_{or}$ to the optical axis.

TABLE 3.6

Focal Lengths and Tilt Angle for the Extreme Ranges of the 4 Subswaths

Subswath Number	$F_{x\,min}$ in mm	$F_{x\,max}$ in mm	Tilt θ of Azimuth Plane	F_r in mm
1	+4804	+4860	+60.4°	-678
2	4860	4915	60.4°	-678
3	4915	4970	60.4°	-678
4	4970	5026	60.4°	-678

The tilt angle θ of the azimuth focal-plane is given by

$$\theta = \tan^{-1}\left[\frac{\lambda_r q}{2p^2\lambda c_a}\right] \tag{3.14}$$

where the positive sense of θ is as shown in Figure 3.5. Note that θ is independent of r_o so that the azimuth focal-plane is flat.

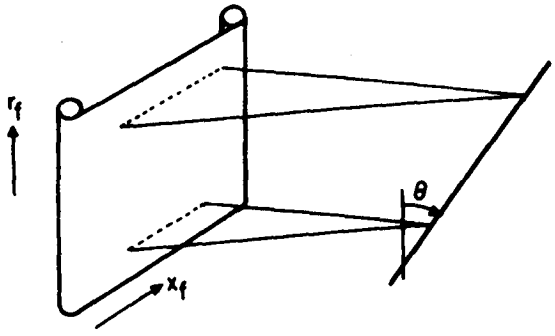

Figure 3.5. Tilt Angle θ of Azimuth Focal-Plane

4. DESCRIPTION OF THE FOURIER TRANSFORM PLANE

4.1 MATHEMATICAL DESCRIPTION

The first lens of a tilted-plane processor is the first spherical lens of the range telescope [3]. At its focal plane is the two-dimensional Fourier transform of the input distribution. At the positive first-order region centred around $f_r = f_{or}$, the amplitude distribution is [2]

$$G_1(f_x,f_r-f_{or}) \simeq c_2\sigma\, F\left[\frac{c(f_r-f_{or})}{2q}\right] e^{-j2\pi(f_r-f_{or})r_o/q}$$

$$h\left[\frac{f_x + 2c_a p/(\lambda_r r_o)[x_{py} + x_{ye}]}{-2c_a p\beta/\lambda_r}\right] e^{\frac{j\pi q r_o f_x^2}{c_a p^2 (f_r+2q/\lambda_r)}}$$

$$e^{-j2\pi f_x x_o/p} \qquad (4.1)$$

where $(f_x,f_r) = (x_2/\lambda F_{s1}, r_2/\lambda F_{s1})$ are the spatial frequencies in azimuth and range respectively

(x_2,r_2) = azimuth and range spatial coordinates in transform plane

λ = wavelength of light used

F_{s1} = focal length of first spherical lens

$f_{or} = f_o/v_c$ cycles/mm = spatial range offset frequency.

Because of the sampling in the input plane, the spectrum is actually the repeated spectrum

$$\sum_{m=-\infty}^{\infty} G_1(F_x - mf_p/v_f,\ f_r-f_{or}); \qquad (4.2)$$

i.e., the spectrum G_1 is repeated at $f_x = \pm mf_p/v_f$.

The presence of the two-dimensional transform within the tilted-plane processor is of great utility for SEASAT-A. As will be seen, doppler-centroid estimation can be performed at this plane. A window can be used at this plane to eliminate all but the m=0 spectrum. Range-curvature correction is best performed at this plane. Finally, division into multiple looks is easily performed at this plane.

4.2 PARAMETERS OF THE FOURIER-TRANSFORM PLANE

As mentioned above, a number of important operations can be performed at the two-dimensional transform plane. This plane is the back-focal plane of the first spherical lens of the range telescope [3]. In this section we determine some of the parameters involved, to aid in the design of frequency-plane operations.

In Figure 4.1 is shown a representation of the spectrum G_1 defined by (4.1) and repeated in azimuth as specified by (4.2). Also present is the complex conjugate of these repeated spectra, located about a centre $f_r = -f_{or}$. Note in (4.1) how pitch and yaw cause the azimuth envelope h, which is actually the two-way antenna amplitude pattern, to shift along f_x. In particular, note that *only* the pattern h shifts, and not the phase functions. In Figure 4.1 the repeated spectra are shown as having sharp and clear boundaries; the boundaries for SEASAT-A spectra, unfortunately, are not sharp and are in fact so indistinct as to cause a serious problem. This subject is discussed further in Section 8.

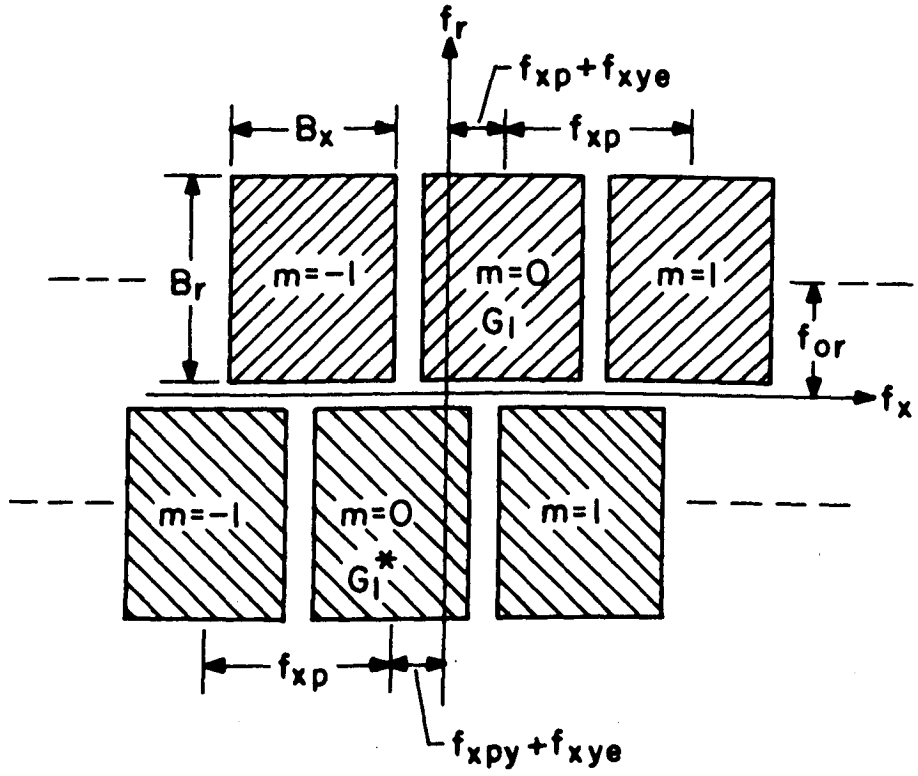

Figure 4.1. Representation of the Two-Dimensional Fourier Transform

The doppler bandwidth is given by

$$\Delta f_d = \frac{2V\beta}{\lambda_r} \tag{4.3}$$

As noted in Table 3.1, it is not clear what value to use for β. For now, we will use β = 16 mrad, so that $\Delta f_d = 2 \times 7.64 \times 10^3 \times 0.016/.235 = 1040$ Hz. Thus, the azimuth bandwidth is

$$B_x = \frac{\Delta f_d}{v_f} = \frac{1040}{40} = 26.0 \text{ c/mm} \tag{4.4}$$

The spectra are separated in azimuth by the spatial PRF

$$f_{xp} = f_p/v_f = \begin{matrix} 36.6 \\ 38.5 \\ 39.5 \\ 41.2 \end{matrix} \quad c/mm$$

It appears that the largest spatial PRF, f_{xp} = 41.2 c/mm, will be used most of the time. From Table 3.5 we saw that f_{or} = 23.2 c/mm and B_r = 38.8 c/mm. The actual spatial dimension in the transform plane is calculated from the spatial frequency with an equation of the form given below (3.6),

$$x_2 = \lambda f_1 f_x \tag{4.5}$$

The focal length f_1 has not been selected yet so Table 4.1 is constructed for 2 different values of f_1:570 mm, which is used on the present DREO correlator, and 784 mm, which is used on the JPL correlator. A wavelength of λ = 632.8 nm is assumed. A spatial frequency f_s corresponds to plane wave being diffracted at an angle

$$\phi_s = \sin^{-1}(\lambda f_s) \simeq \lambda f_s \tag{4.6}$$

to the optical axis. The angles ϕ_{xp} and ϕ_{or} corresponding to offset frequencies f_{xp} and f_{or} are given in Table 4.1.

TABLE 4.1

Spatial Dimension and Angle of Various Spatial-Frequency Parameters

	Spatial Frequency in c/mm	Distance in mm for f_1 = 570 mm	Distance in mm for f_1 = 784 mm	Wave Angle
f_{xp}	41.2	14.9	20.4	1.49°
B_x	26.0	9.0	12.4	
f_{or}	23.2	8.4	11.5	0.84°
B_r	38.8	12.2	19.3	

The offset of the envelope h because of pitch, yaw, and equivalent yaw is

$$f_{xpy} + f_{xye} = \frac{2c_a p}{\lambda_r r_o} (x_{py} + x_{ye}) \tag{4.7}$$

which, in terms of time frequency, is

$$f_{py} + f_{ye} = \frac{2V}{\lambda_r r_o} (x_{py} + x_{ye}) \tag{4.8}$$

Values of x_{py} and x_{ye} in Table 3.2 are converted to their equivalent frequency, spatial frequency, and wave angle and are tabulated in Table 4.2. Values of λ = 632.8 nm and f_1 = 570 mm were used.

TABLE 4.2

Selected Values for f_{py} and f_{ye} and their Spatial Equivalents

	$\phi_o = 30.6°$ $r_o = 860$ km	$\phi_o = 73.8°$ $r_o = 860$ km	$\phi_o = 52.5°$ $r_o = 841$ km	$\phi_o = 52.5°$ $r_o = 860$ km	$\phi_o = 52.5°$ $r_o = 879$ km
f_{py} Hz	741	741	719	741	755
f_{ye} Hz	1391	454	843	982	1102
f_{xpy} c/mm	18.5	18.5	18.0	18.5	18.9
f_{xye} c/mm	34.8	11.3	21.1	24.6	27.6
$f_{xpy}\lambda f_1$ mm	6.7	6.7	6.5	6.7	6.8
$f_{xye}\lambda f_1$ mm	12.6	4.1	7.6	8.9	10.0
ϕ_{py}	0.67°	0.67°	0.65°	0.67°	0.69°
ϕ_{ye}	1.26°	0.41°	0.77°	0.89°	1.00°

Upon comparing the offsets in Table 4.2 to the values of the frequency plane parameters given previously, it can be seen that spectra can be offset more than one PRF distance. For example, in the worst-case combination shown in Table 4.2, an offset of 53.3 c/mm (2132 Hz) occurs. Compare this to the maximum PRF of 41.2 c/mm (1647 Hz). Also note that the shift is dependent on range. For example, at ϕ_o = 52.5°, the worst-case shift varies by 7.4 c/mm (295 Hz) between the minimum and maximum range. Since in the two-dimensional transform plane the spectra from targets at different ranges are superimposed, an effective broadening of the total spectrum takes place, making it more difficult to distinguish between two repeated spectra. This subject is discussed further in Section 8.

4.3 EFFECTS OF NON-ZERO SAMPLE WIDTH

In (3.1) the azimuth sampling function, which samples at the PRF, is shown as a δ function. In practice the sample width is non-zero and is determined by the azimuthal spread of the CRT spot size. Thus, at the interferogram,

the samples will be partially overlapping [1]. In heavily over-sampled SAR's, such as the ones used at ERIM, overlapping can actually be beneficial both by increasing the exposure of the recording film and by low-pass filtering to eliminate higher-order spectra. For SEASAT-A the sampling rate is barely twice the azimuth bandwidth, so that overlapping is detrimental. The effects of the non-zero sample width on the azimuth spectrum will now be considered.

The CRT spot is usually gaussian in intensity so that the intensity exposing the film is

$$I = I_{of}\, e^{-2.77\, x_f^2/w_f^2} \tag{4.9}$$

where I_{of} is the intensity at the centre of the light spot at the film and w_f is the spot width at the half-intensity level. It is assumed that the linear portion of the t_a-E film exposure response is employed, so that the amplitude transmittance, t_a, is proportional to the exposure $E = It_e$, where t_e is exposure time. Thus, on the developed film, the spot has the shape

$$t_a(x_f) = t_{ao}\, e^{-2.77\, x_f^2/w_f^2} \tag{4.10}$$

where t_{ao} is a constant depending on I_{of}. If the δ function is replaced by $t_a(x_f)$ of (4.10) and the two-dimensional Fourier transform performed, then it can be shown that the amplitude of the spectrum becomes

$$G_1'(f_x, f_r - f_{or}) = e^{-3.56\, w_f^2 f_x^2} \sum_{m=-\infty}^{\infty} G_1(f_x - mf_{xp}, f_r - f_{or}) \tag{4.11}$$

where constants in front of the exp function have been omitted. The effect of non-zero sample width is the addition of a weighting function which is just the transform of the spot shape (4.10). Thus, the wider the spot width w_f, the narrower the weighting function will be. This weighting function is shown in Figure 4.2 as a function of the dimensionless quantity $w_f x_f$. For the SEASAT-A recorder a CRT spot size of about 0.7 mil will be used. This will be reduced by 1.36 times onto the film so that $w_f = 0.0007 \times 25.4/1.36 = 1.3. \times 10^{-2}$ mm. A second abscissa scale is provided in Figure 4.2 as a function of f_x alone for the case where $w_f = 13.1$ μm.

There are also superimposed in Figure 4.2 the repeated spectra ΣG_1. Their exact shape would again be the two-way antenna amplitude pattern. Although only an approximate shape has been sketched, the half-intensity width of 26.0 c/mm given in Table 4.1 was maintained. Furthermore, each order has been drawn in Figure 4.2 as though it were separate from all other orders. In reality the total spectrum is a sum of all the spectral orders so that the dip between peaks is much less pronounced than the dip shown. It is the author's opinion that, at the time of writing, it is not known how well each order is

distinguishable from another, but some study is continuing on this subject both at MacDonald, Dettwiler and Associates Ltd. and at Queen's University.

In Figure 4.2 the m=0 spectrum is centred on f_x=0, which implies no combined pitch, yaw and equivalent yaw. The weighting function would not deteriorate the m=0 spectrum much. However, the m=0 spectrum being centred on f_x=0 would occur very rarely for SEASAT-A. In Figure 4.3 is shown a worst-case offset, which from Table 4.2 is $f_{xpy}+f_{xye}$ = 53.3 c/mm. The shifted but unweighted spectra are shown as solid lines. Their shapes after weighting are shown by dotted lines. The m=0 spectrum is seriously degraded so that it likely cannot be used (see Section 7). Furthermore, the problem of doppler-centroid estimation is made much more difficult (see Section 8).

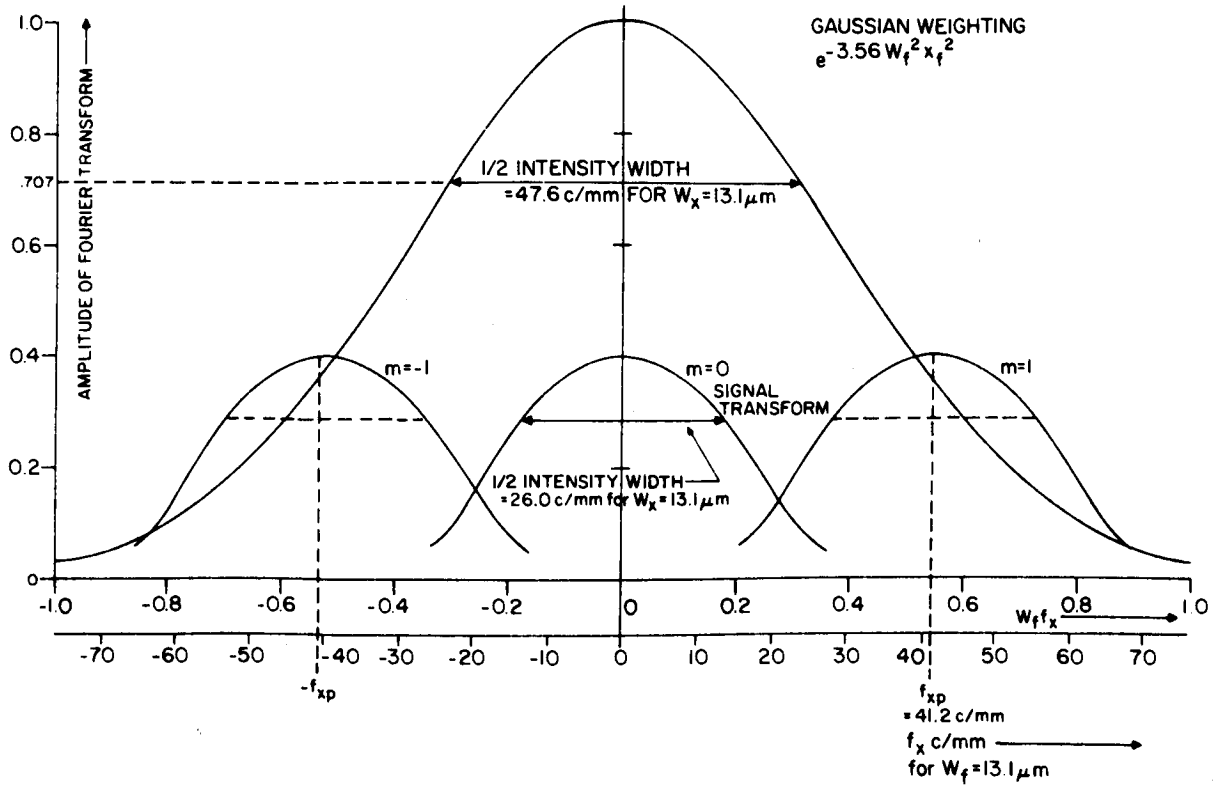

Figure 4.2. Amplitude of weighting function vs $W_f f_x$ and vs f_x for W_f = 13.1 μm. The repeated transforms of the signal for no pitch and yaw are also given.

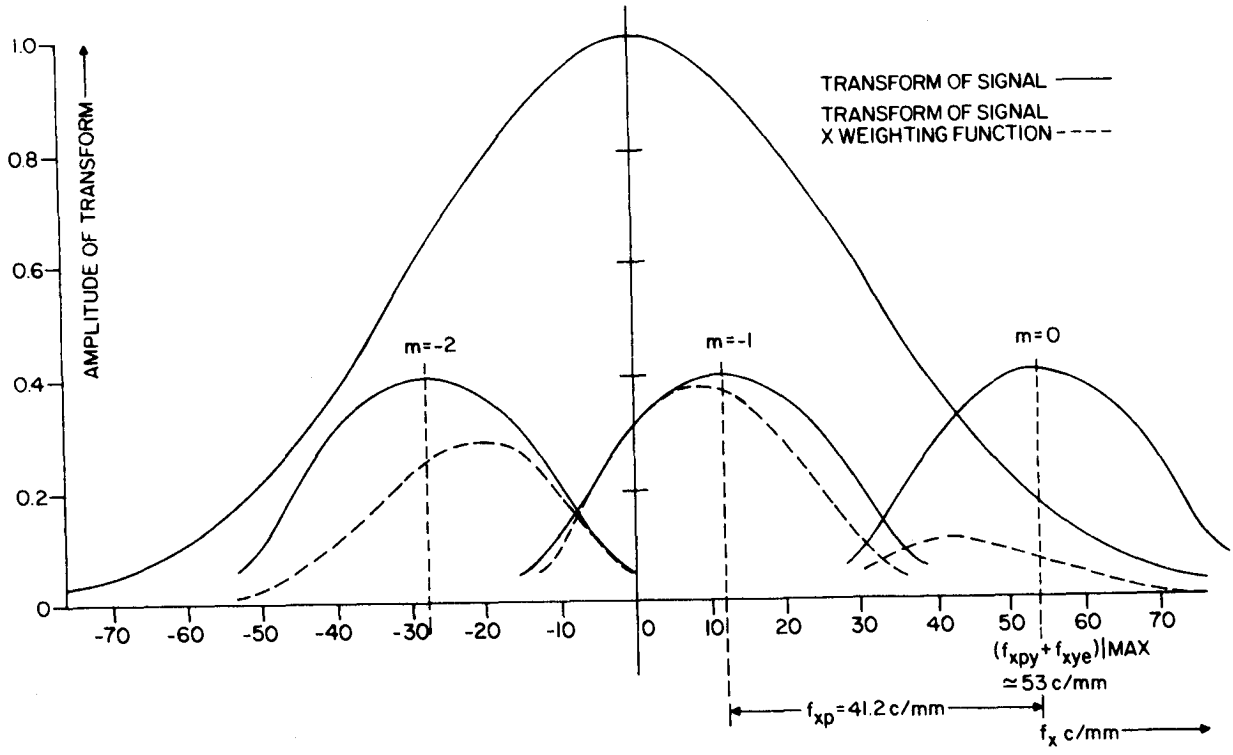

Figure 4.3. Amplitude of the transform vs f_x for W_f = 13.1 μm. for maximum pitch, yaw and equivalent yaw. The dashed lines give the actual pattern obtained, i.e. the transform X weighting function.

5. BASIC CORRELATOR

In Section 3.4, it was seen that illumination of the interferogram with plane-wave light results in an erect range-image on one side of the interferogram, and an azimuth-image on the other side tilted at an angle θ as shown in Figure 3.5. The object of the tilted-plane processor is to take these two non-parallel planes, make them parallel, and then superimpose them to produce a two-dimensional image. Furthermore, it is desired to make the aspect ratio unity.

There are three features an optical processor can have that are desired for the SEASAT-A processor. The first, called *tracking*, is an inherent feature of tilted-plane processors. By tracking is meant that the output recording film can be moved in synchronism with the interferogram. The tracking feature follows from the fact that the instantaneous output image is of large extent in both dimensions. Thus static "snap shot" images may be obtained as has always been done on the present DREO correlator. However, by moving the output recording film in synchronism with the interferogram, continuous multiple exposures are made on the output film and laser speckle is greatly reduced.

The second feature the processor may also possess is *decoupling*, which means that range and azimuth adjustments can be made independently of each other. The third feature a processor may have is a variable magnification capability in one dimension, which means that the aspect ratio can be varied over a certain range.

A basic tilted-plane optical correlator having the decoupling and variable magnification features is shown in Figure 5.1. The two spherical lenses L_{s1} and L_{s2}, separated by the sum of their focal lengths, form the range telescope. If the focal lengths are equal ($f_1 = f_2$), then range magnification $M_r=1$. The azimuth telescope consists of cylindrical elements, which have optical power in the azimuth direction only. With this combination of range and azimuth telescopes, the range and azimuth focussing can be performed independently, and are thus decoupled. Because there are three lenses in the azimuth telescope, the azimuth magnification can be varied by varying the lens spacing.

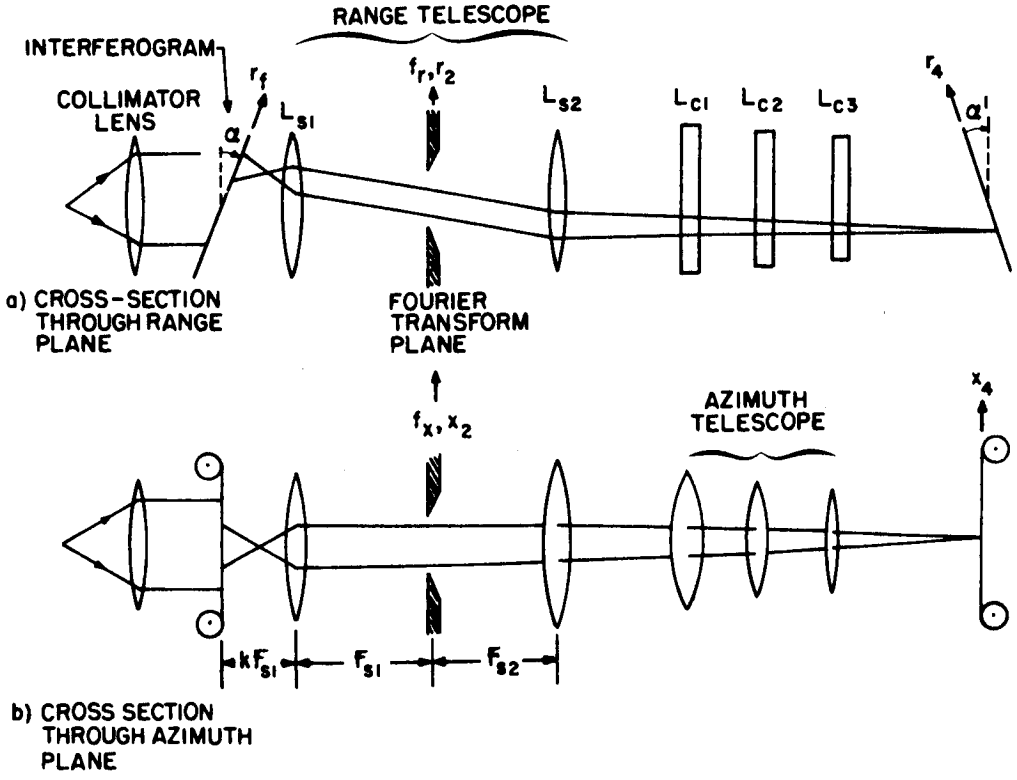

Figure 5.1. Basic Decoupled Tilted-Plane Processor with Variable Aspect Ratio

To compensate for the tilt of the azimuth image, the r_f axis of the interferogram film is tilted by an angle α and the output recording film is tilted by an angle α', as shown.

5.1 INCIDENCE ANGLES

In (4.1) it is seen that the spectrum is offset in range frequency by the spatial range-offset frequency f_{or}. Also the envelope of the spectrum is offset in azimuth frequency by $f_{xpy}+f_{xye}$, given by (4.7), because of pitch, yaw, and equivalent yaw.

To reduce the frequency response requirements of the optical system, it is desired to eliminate such offsets, so that the ray bundles propagate along the optical axis. In this subsection the range offset is considered; the azimuth offsets are considered in Section 7.

As illustrated in Figure 5.2(a), plane-wave light propagating parallel to the optical axis of the lens L_{s1} is incident on the interferogram. The interferogram is tilted at an angle α. To the right of the interferogram three beams exist: the dc or "straight-through" beam, the positive first-order signal beam, and the negative first-order signal beam. As will be discussed in Section 5.3, it is likely the positive first-order beam that will be used. This beam diverges from the optical axis at an angle

$$\sin\theta_r \simeq \theta_r = \lambda f_{or} \tag{5.1}$$

which for SEASAT-A is $\sin^{-1}(23.2 \times 0.6328 \times 10^{-3}) = 0.84°$. Some of the light of this order misses the aperture of lens L_{s1}. To remedy this problem, the incident light is inclined at an angle θ_r as shown in Figure 5.2(b). The first order beam now propagates parallel to the optic axis of lens L_{s1} and is centred on the optic axis so that the full aperture of L_{s1} is utilized. The spectrum at the transform plane changes from $G_1(f_x,f_r-f_{or})$ given by (4.1) to $G_1(f_x,f_r)$.

The adjustment of the angle of inclination is usually implemented in conjunction with a corner-turning mirror. Usually the corner turning is done with respect to the azimuth angle as shown in Figure 5.3. Then the mirror must be rotatable about the axis shown. The inclination adjustment may be done before the interferogram as shown; this approach is used by JPL. Alternatively, it may be done just after the interferogram, as at ERIM. The method presently used at DREO, where the adjustment is made after the lens L_{s1}, is not recommended. It is suggested for the new DREO correlator that the adjustment be made before the interferogram, as at JPL.

5.2 ASPECT RATIO AND TILT ANGLES

Aspect ratio considerations were discussed at length in [1]; relevant details are reviewed here and specific values are updated. Aspect ratio is defined as the ratio of the azimuth-dimension scale to the range-dimension scale. If

$$m_a = 1/p = \text{azimuth magnification of recording}$$

and

$$m_r = 1/q = \text{range magnification of recording}$$

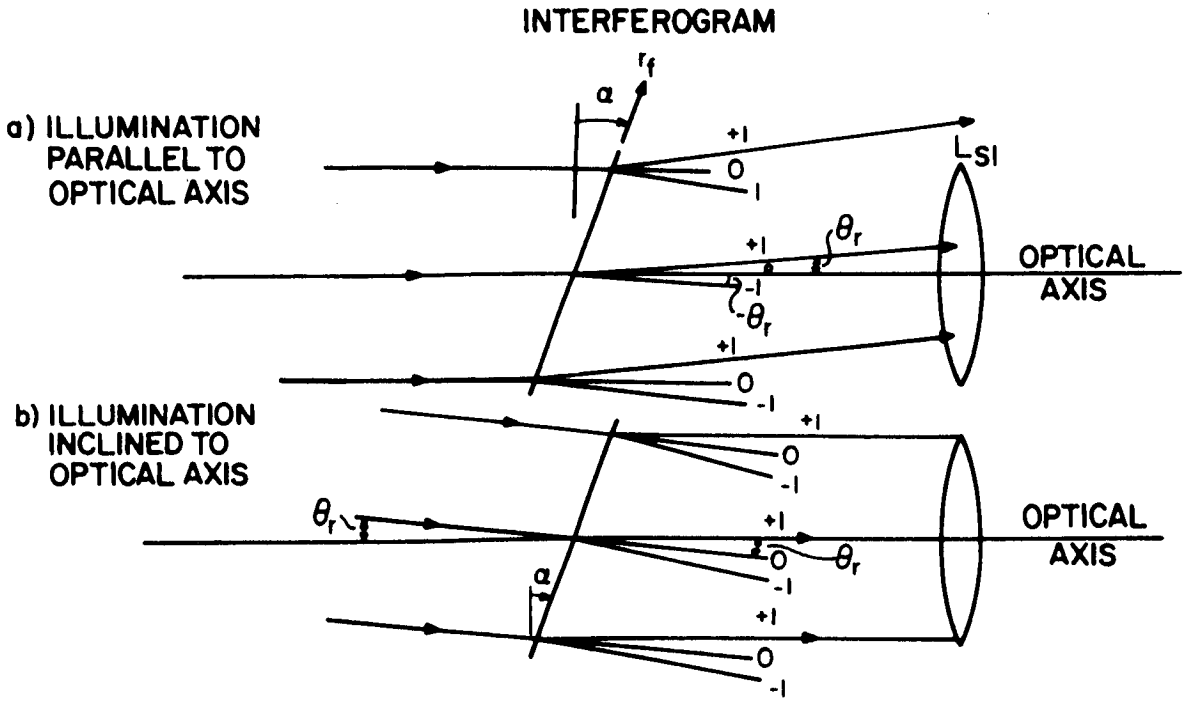

Figure 5.2. Tilting Incidence Angle for Range Dimension

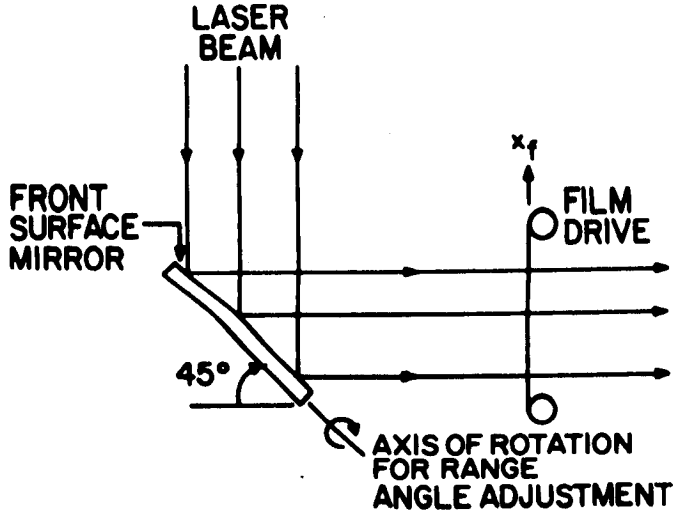

Figure 5.3. Corner Turning Mirror with Adjustment of Range Incidence Angle

then the aspect ratio A_F of the interferogram film is

$$A_f = \frac{m_a}{m_r} = \frac{q}{p} , \tag{5.2}$$

which is called the "K" value in [3]. The optical correlator has magnifications

M_r = range magnification (usually = 1),

M_a = azimuth magnification

so that the aspect ratio of the optical correlator is

$$A_o = \frac{M_a}{M_r} \tag{5.3}$$

A "K" value may also be defined for the correlator as $K_o = 1/A_o$.

The tilt angle θ of the azimuth image is shown in Figures 3.5 and 5.4(a) and given by (3.14). The azimuth output image is tilted at an angle [3]

$$\tan\beta = -(\tan\theta)A_o^2 . \tag{5.4}$$

Thus for $A_o < 1$ there is a reduction in the angle β.

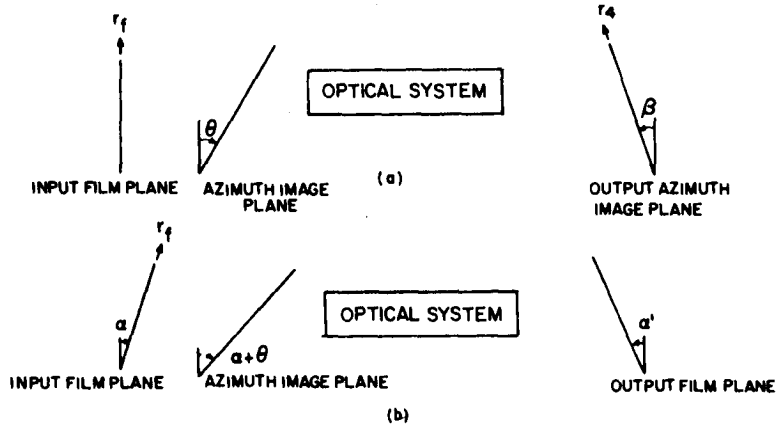

Figure 5.4. Tilt Angles (a) before Tilting Film Plane and (b) after Tilting Film Plane

If the film plane is tilted at an angle α as shown in Figures 5.1(a) and 5.4(b), then the output range and azimuth image planes can be made coincident and are tilted at an angle α', found from

$$\tan\alpha' = -\tan(\theta+\alpha)A_o^2. \tag{5.5}$$

If the range telescope is adjusted to have unity magnification then

$$\alpha' = -\alpha \tag{5.6}$$

and

$$-\tan\alpha = -\tan(\theta+\alpha)A_o^2. \tag{5.7}$$

The required tilt angle α can be found iteratively.

For practical reasons, it is desired to keep α as small as possible. It is kept small by a suitable choice of A_o. If A_o is small then (5.7) can be approximated by

$$\alpha \simeq (\alpha + \tan\theta)A_o^2 \tag{5.8}$$

which from (3.14) leads to

$$\alpha \simeq \frac{A_o^2}{1-A_o^2}\left[\frac{\lambda_r q}{2p^2\lambda c_a}\right] = \frac{A_o^2}{1-A_o^2}\frac{\lambda_r A_f}{2p\lambda c_a}. \tag{5.9}$$

If the value of α calculated from (5.9) is not sufficiently accurate for a particular case, it still provides a good initial value for the iterative solution of (5.7).

In Section 3.4 it is seen that $\theta = 60.4°$ so that α and α' could be very large - a highly undesirable feature in a practical system. The angle β in (5.4) can be greatly reduced by making A_o very small. However the film aspect ratio $A_f = 1.81$ indicates that an optical system aspect ratio of $A_o = 1/A_f = 0.55$ would be necessary to give unity output aspect ratio with respect to slant range. Then, $\beta = -28.0°$, still undesirably large.

Slant-range-to-ground-range conversion was seen in Section 3.2 to be approximately a simple magnification of the slant range by M_{rc}. This conversion can be combined with the normal operation of the correlator. Since it is desired to keep the range telescope at unity magnification, the magnification M_{rc} in slant range is realized instead as a demagnification $1/M_{rc}$ in azimuth. Therefore, for unity aspect ratio in ground range, it is required that

$$A_f A_o = \frac{m_a}{m_r} \frac{M_a}{M_r} = \frac{1}{M_{rc}} \tag{5.10}$$

so that

$$A_o = \frac{1}{A_f M_{rc}} = \frac{1}{K_o} . \tag{5.11}$$

The values of A_o required to produce unity aspect ratio in ground range are given in Table 5.1 for the 4 subswaths of Figure 3.1. The angles β and α are also given, and show that the tilts have been brought down to a reasonable practical magnitude.

TABLE 5.1

Values of A_o, K_o, β and α for the 4 Subswaths that Lead to Unity Output Aspect Ratio in Ground Range

Subswath Number	M_{rc}	A_o	K_o	β	α
1	2.916	0.190	5.28	3.6°	3.8°
2	2.670	0.207	4.83	4.3°	4.5°
3	2.483	0.223	4.49	5.0°	5.3°
4	2.336	0.237	4.23	5.7°	6.0°

5.3 IMAGE SELECTION AND SHIFT LENS

The focal lengths of the interferogram are given in Table 3.6. This table shows that the azimuth image is focussed at about 4.9 m on one side of the interferogram, and the range image is focussed at about 0.7 m on the other side. At JPL, the real azimuth image and the virtual range image will be utilized. Unless good reasons arise otherwise, it is sensible to utilize the same combination for the DREO correlator. This implies that the positive first order in range is to be used.

The locations of these images, due to the magnitudes of these focal lengths, are inconvenient for good correlator design. The image planes may be moved to more favorable locations by means of a shift lens. The shift-lens technique appears to have been developed at Goodyear Aerospace. JPL will be making use of the method in processing SEASAT-A data. A brief description of the operation of a shift lens is now given.

In the telescopic system of Figure 5.5(a) the image position is

$$z_i = -(F_2/F_1)^2 z_o \tag{5.12}$$

where z_o is the object distance measured from the focal point of lens L_{s1} and z_i is the image distance. For Figure 5.5(a), z_o is negative and z_i is positive. The lateral magnification is

$$m_x = -(F_2/F_1) \tag{5.13}$$

and the longitudinal magnification is

$$m_z = -(F_2/F_1)^2. \tag{5.14}$$

Suppose a lens L_s of focal length F_s is placed at the common focal plane of L_{s1} and L_{s2}. From [3] it can be shown for such a 3-lens system that

$$z_i = -(F_2/F_1)^2 z_o - F_2^2/F_s \tag{5.15}$$

and that this system has lateral and longitudinal magnification, respectively,

$$m_{xs} = -(F_2/F_1) \tag{5.16}$$

and

$$m_{zs} = -(F_2/F_1)^2. \tag{5.17}$$

Thus the shift lens has not had any effect on lateral or longitudinal magnification so that image size, shape and tilt are unaltered. The only effect, as can be seen from (5.15), is to shift the image a distance

$$\Delta z_i = + F_2^2/F_s \tag{5.18}$$

where the positive sign indicates a shift to the left. By writing (5.15) as

$$z_o + \frac{F_1^2}{F_s} = -\left[\frac{F_1}{F_2}\right]^2 z_i \tag{5.19}$$

we see that the use of a shift lens is the equivalent of shifting the object by a distance

$$\Delta z_o = + F_1^2/F_s \tag{5.20}$$

where again the positive sign indicates a shift to the left.

For the JPL system, a shift lens is being constructed that on one side is a negative spherical lens and on the other side is a positive cylindrical lens with its focussing power in azimuth. The overall effect is to produce a negative cylinder in range and a positive cylinder in azimuth. Then the

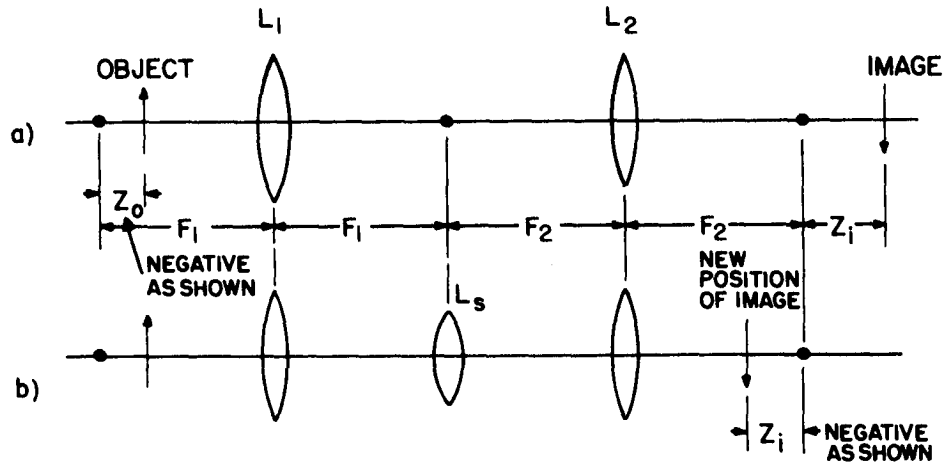

Figure 5.5. Two Lens Telescope (a) Without a Shift Lens and (b) With a Shift Lens

virtual range image is shifted to the right and thus becomes equivalent to a real image (i.e., to the right of the interferogram) and simultaneously, the real azimuth image, with a natural focal length of about 4.9 m, is brought closer to the interferogram.

6. CORRECTION FOR PITCH AND YAW

6.1 USE OF THE ZERO-ORDER AZIMUTH SPECTRUM

As can be seen in Figure 4.1, the desired zero-order azimuth spectrum $G_1(f_x,f_r-f_{or})$, which becomes $G_1(f_x,f_r)$ after range inclination-angle adjustment, is offset in the f_x dimension because of antenna pointing-angle error (pitch, yaw, and equivalent yaw). The angular offsets ϕ_{py} and ϕ_{ye} are given by (4.6) and (4.7), and selected values are given in Table 4.2. Such offsets greatly increase the spatial-frequency response requirements for the correlator. For example, it is seen from Tables 4.1 and 4.2 that, with no pitch and yaw, the spectrum would occupy a width in the transform plane between $x_2 = \pm 4.5$ mm if $F_{s1} = 570$ mm. But with pitch and yaw, the extreme edges could be located anywhere within a width of about ±24 mm. At the input plane, a signal extending between $x_f = \pm 80.5/2 = \pm 40.3$ mm (see Table 3.5) could be offset in x_f by up to ±170 mm. Obviously an input-plane aperture of over 300 mm is impractical. If one attempts to directly correlate the signal while it is centred in the input aperture, the output is shifted by a similar amount, which makes the optics for the output stage equally impractical.

In Figure 6.1 is represented the situation where the envelope h of the signal g given by (3.1) is centred in the input aperture. Since x_{py} and x_{ye}

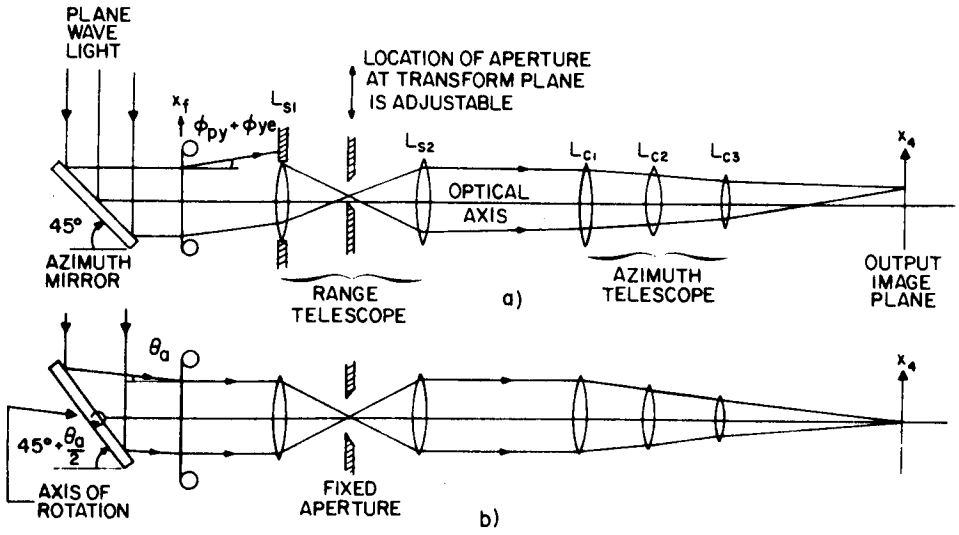

Figure 6.1. End-to-End Azimuth Cross-Section for One Range with (a) Azimuth Mirror at 45° and (b) Azimuth Mirror Adjusted to Compensate for Pitch and Yaw

are functions of range, the function h cannot be centred for all values of r_o at once. For this discussion then, it is assumed that the envelope h is centred for $r_o = r_{oav}$, the average range. This form of centering means that the azimuth phase function in (3.1) becomes

$$\exp -j \frac{4\pi c_a p^2}{\lambda_r 2 r_o} \left[x_f - \frac{x_o + x_{pya} + x_{yea}}{p} \right]$$

where x_{pya} and x_{yea} are the offsets x_{py} and x_{ye} for $r_o = r_{oav}$. Thus the phase function, instead of being centred on $x_f = x_o/p$, is centred on

$$x_f = \frac{x_o + x_{pya} + x_{yea}}{p}. \tag{6.1}$$

In this case and for Figure 6.1(a) where the azimuth turning mirror is set at 45°, the output azimuth image is located at

$$x_4 = \frac{M_a}{p} (x_o + x_{pya} + x_{yea}) \tag{6.2}$$

where x_4 is the azimuth dimension in the output plane, measured from the optical axis, and M_a is the azimuth-dimension magnification. (Recall that $M_a<1$). Output location (6.2) is, of course, the one for correct mapping of

the input signal whose phase is centred according to (6.1). Now the principal axis of the first-order (signal) wave is inclined to the optical axis at an angle $\phi_{py} + \phi_{ye}$, given by the small angle approximation in (4.6) and (4.7) to be

$$\phi_{py}(r_o) + \phi_{ye}(ro) = \frac{2c_a p\lambda}{\lambda_r r_o} [x_{py}(r_o) + x_{ye}(r_o)]. \tag{6.3}$$

These angles are nonlinear functions of r_o. As discussed above, this inclination causes practical difficulties. As illustrated in Figure 6.1(a), part of the propagating wave is blocked by the limiting aperture of the lenses. The spectrum is offset, so the aperture at the transform plane must be shifted appropriately to track the spectrum as pitch and yaw changes.

To alleviate this problem, suppose the azimuth mirror is rotated about the axis shown in Figure 6.1(b) by an extra amount $\theta_a/2$ so that the angle of incidence on the interferogram is θ_a. This corresponds to multiplying the input function (3.1) by $\exp[-j2\pi\sin\theta_a(x_f/\lambda)]$. If θ_a is chosen so that

$$\theta_a = \phi_{py}(r_{oav}) + \phi_{ye}(r_{oav}) \tag{6.4}$$

then for $r_o = r_{oav}$, the first order wave will propagate parallel to the optical axis of the lens, making optimum use of the available aperture. Furthermore, the spectrum will be centred on $f_x=0$ at the transform plane. For values of $r_o \neq r_{oav}$ there will be some small inclination to the optical axis and some small offset in the transform plane.

Because of the inclination θ_a, the azimuth focus of the interferogram, as described in Section 3.4, will be offset in the azimuth dimension by a distance

$$\Delta x_1 = -F_x \sin\theta_a \simeq -F_x\theta_a = -\frac{\lambda_r r_o \theta_a}{2p^2\lambda c_a} \tag{6.5}$$

where F_x is the azimuth focal-length given by (3.12). The output image will be located at

$$\begin{aligned} x_4 &= \frac{M_a}{p}(x_o + x_{pya} + x_{yea}) - \frac{M_a\lambda_r r_o\theta_a}{2p^2\lambda c_a} \\ &= \frac{M_a}{p}x_o + \frac{M_a}{p}(x_{pya} + x_{yea})\left[1 - \frac{r_o}{r_{oav}}\right] \end{aligned} \tag{6.6}$$

which is the desired location $M_a x_o/p$ plus a small offset. This offset is zero at $r_o = r_{oav}$ but is range dependent elsewhere so that the output image is distorted. For a maximum value for $x_{pya} + x_{yea}$ of approximately 28.2 km, from Table 3.4, the distortion Δx_4 between maximum and minimum range for subswath 2 is

$$\frac{(x_{pya} + x_{yea})}{r_{oav}} (r_{omax} - r_{omin}) = 320 \text{ m}$$

or 320/25 = 13 resolution cells. This expression is in units of the object coordinate and is obtained from the azimuth dimension x_4 by multiplying by p/M_a. Thus, a worst-case azimuth distortion with respect to the azimuth position for r_{sav} is about ±7 resolution elements.

It is fairly simple to eliminate this distortion by rotating the output recording device by an angle γ_a about the axis perpendicular to the output plane at the point $(x_4,r_4) = (0,r_{oav}/q)$. For γ_a and x_4 small, the new coordinates in terms of the old are $(x_4',r_4') = [x_4 + (r_4 - r_{oav}/q)\gamma_a, r_4]$. If γ_a is chosen according to

$$\frac{\gamma_a r_{oav}}{q} \left[\frac{r_4 q}{r_{oav}} - 1\right] = \frac{M_a}{p} (x_{pya} + x_{yea}) \left[\frac{r_o}{r_{oav}} - 1\right] \tag{6.7}$$

so that

$$\gamma_a = \frac{qM_a}{pr_{oav}} (x_{pya} + x_{yea}) = \frac{qM_a \lambda r}{2c_a p^2 \lambda} \theta_a, \tag{6.8}$$

then this distortion is eliminated. Note that γ_a must be varied as offsets $x_{pya}+x_{yea}$ vary. As an example, consider subswath 2 with $M_a = A_o = 0.207$ and, from Table 3.3, a worst-case combination of $x_{pya}+x_{yea}$ of about 20 km. Then $\gamma_a = 8.8$ mrad = 0.5°.

It appears that JPL will correct the distortion by employing a corner turning mirror placed between the azimuth telescope and the output plane. The mirror's angle is adjusted so as to cancel the distortion by rotation of the tilted output plane. Unfortunately, this technique adds an extra, constant azimuth shift that varies with $x_{pya}+x_{yea}$ and that must be accounted for.

In Table 6.1 are summarized both the form of the azimuth functions and the azimuth position of the three azimuth image planes. The three image planes are: 1) the azimuth image of the interferogram located a distance $\pm F_x$ from the interferogram, 2) the azimuth image, a distance $\pm F_{fx}$ from the transform plane, and finally 3) the output image itself. The first row is for the phase function centred on $x_f = x_o$ and normal illumination. In the next row, the input film is shifted so that envelope h is centred on $x_f = x_o/p$, but

illumination is still normal to the film. In the third row, the illumination is tilted. The transform plane functions and offsets will be useful in Section 7, where effects on range-curvature correction are considered.

6.2 USE OF OTHER AZIMUTH SPECTRAL ORDERS

In Section 4.3 it was seen, as shown in Figure 4.2, that the zero-order azimuth spectrum badly deteriorates as pitch and yaw increase. It was suggested by JPL that, as the zero-order spectrum moves out of the region near $f_x=0$, the order moving into the region $f_x=0$ be used for the processing instead. It is now considered how such a non-zero-order spectrum can be utilized.

It is assumed that if the zero-order azimuth spectrum (see Figure 4.2) shifts by just slightly more than $+f_{px}/2$, then the -1 order is selected for use. Therefore there is a switch from spectrum $G_1(f_x,f_r)$ given by (4.1) to $G_1(f_x + f_{xp},f_r)$. The azimuth-frequency dependent portion is

$$G_1(f_x-f_{xp}) = c_5\, h\left[\frac{f_x + f_{xpy} + f_{xye} + f_{xp}}{-2c_a p\beta/\lambda_r}\right]$$

$$e^{j\frac{\pi q r_o (f_x-f_{xp})^2}{c_a p^2 (f_r+2q/\lambda_r)}} \qquad e^{-j2\pi(f_x-f_{xp})x_o/p}. \qquad (6.9)$$

This shift is equivalent to a tilt $\phi_p = \lambda f_{xp}$ at the interferogram plane. Thus, for the mirror at 45° as in Figure 6.1(a), the same reasoning as used for (6.5) and (6.6) may be used to obtain the output position as

$$x_4 = \frac{M_a x_o}{p} - \frac{M_a \lambda r_o \phi_p}{2c_a p^2 \lambda}\,. \qquad (6.10)$$

The extra offset is range dependent. Once again it is possible to tilt the mirror, this time to centre the -1 order spectrum. Angle θ_{a1} is chosen now so that

$$\theta_{a1} = \phi_{py}(r_{oav}) + \phi_{ye}(r_{oav}) - \phi_p. \qquad (6.11)$$

Note that the switch from the 0 order to the -1 order logically should occur when

$$\phi_{py}(r_{oav}) + \phi_{ye}(r_{oav}) = \phi_p/2\,. \qquad (6.12)$$

At that instant θ_a should change from $\phi_p/2$ to $-\phi_p/2$.

TABLE 6.1

Azimuth functions at input and transform planes plus azimuth position at other planes for various input positions and illumination angles

SET UP	INPUT AZIMUTH FUNCTION	AZIMUTH LOCATION OF INPUT AZIMUTH FOCAL LINE x_1	TRANSFORM PLANE AZIMUTH FUNCTION $f_x = x_2/F_{s1}$	AZIMUTH LOCATION OF TRANSFORM PLANE AZIMUTH LINE FOCUS x_3	AZIMUTH LOCATION OF OUTPUT IMAGE x_4
Phase function centered on $x_f=x_o$, illumination at normal incidence.	$h'[x_f-x_o+x_{py}+x_{ye}]$ $\exp -j\frac{2c_a p}{r r_o}(x_f-x_o/p)$	x_o/p	$h''(f_x+f_{xpy}+f_{xye})$ $\exp \frac{j q r_o f_x}{c_a p^2(f_r+2q/r)}$ $\exp -j2f_x x_o/p$	$\frac{F_{fx}x_o}{F_{s1}p}$ $\frac{-2pc_a F_{s1}x_o}{r_o r}$	$\frac{M_a x_o}{p}$
Input function shifted so that envelope h is centered on $x_f=x_{o/p}$, illumination at normal incidence.	$h'(x_f-x_o/p)$ $\exp -j\frac{2c_a p}{r r_o}\left[x_f-\frac{x_o+x_{pya}+x_{yea}}{p}\right]$	$\frac{x_o+x_{pya}+x_{yea}}{p}$	$h''(f_x+f_{xpy}+f_{xye})$ $e^{\frac{j q r_o f_x}{c_a p(f_r+2q/r)}}$ $e^{j2f_x\left[\frac{x_o+x_{ypa}+x_{yea}}{p}\right]}$	$\frac{F_{fx}}{F_{s1}p}(x_o+x_{ypa}+x_{yea})$	$\frac{M_a}{p}(x_o+x_{pya}+x_{yea})$
Input function shifted so that envelope h is centered on $x_f=x_{o/p}$, illumination inclined at angle γ_a given by (7.4)	$h'(x_f-x_o)$ $\exp -j\frac{2c_a p}{r r_o}\left[x_f-\frac{x_o+x_{pya}+x_{yea}}{p}\right]$ $\exp -j2(f_{pya}+f_{yea})x_f/$	$\frac{x_o+x_{pya}+x_{yea}}{p}$ $-\frac{r_o}{r_{oav}}\left[\frac{x_{pya}+x_{yea}}{p}\right]$	$h''(f_x)$ $e^{\frac{j q r_o(f_x-f_{apy}-f_{aye})}{c_a p(f_r+2q/r)}}$ $e^{j2(f_x-f_{apy}-f_{aye})\left[\frac{x_o+x_{pya}+x_{yea}}{p}\right]}$	$\frac{F_{fx}}{F_{s1}p}(x_o+x_{pya}+x_{yea})$ $-F_{s1}(f_{apy}+f_{aye})$ $=\frac{F_{fx}}{F_{s1}p}x_o$ $+\frac{F_{fx}-F_{fxav}}{F_{s1}p}$ $(x_{pya}+x_{yea})$	$\gamma_a = 0$ $\frac{M_a}{p}x_o$ $+\frac{M_a}{p}(x_{pya}+x_{yea})\left[1-\frac{r_o}{r_{oav}}\right]$ $\gamma_a = (6.8)$ $\frac{M_a}{p}x_o$

NOTES:
1. h' and h" are abbreviated forms of h wherein constants have been absorbed.
2. Purely range - dependent functions have been omitted.
3. x_{py}, x_{ye}, f_{xpy} and f_{xye} are meant as functions of range r_o whereas x_{pya}, x_{yea}, f_{apy} and f_{aye} are the values for r_{oav}.
4. We have used $x_{py}-x_{pya}+x_{ye}-x_{yea}=0$ in h' and $f_{xpy}-f_{apy}+f_{xye}-f_{aye}=0$ in h" because the exact position of the envelope has little influence on the points being illustrated.

Again consider the envelope h in the interferogram to be centred in the input aperture so that the azimuth phase function is centred on

$$x_f = x_o + x_{pya} + x_{yea}. \tag{6.13}$$

The output azimuth signal is located at

$$x_4 = \frac{M_a}{p}[x_o + x_{pya} + x_{yea}] - \frac{M_a \lambda r_o(\theta_{a1} + \phi_p)}{2p^2 \lambda c_a} \tag{6.14}$$

which from (6.11) becomes

$$x_4 = \frac{M_a}{p} x_o + \frac{M_a}{p}(x_{pya} + x_{yea})\left[1 - \frac{r_o}{r_{oav}}\right] \tag{6.15}$$

which is exactly the same as for the 0 order case given by (6.6). To eliminate the range dependent term that causes distortion, angle γ_a is set as for the 0 order case so that γ_a is given by (6.8). Thus, at switch over, when (6.12) holds, the rotation angle γ_a of the output plane is *not* changed.

In general, a distortion free image may be obtained from the n^{th} order provided the azimuth mirror is set so that

$$\theta_{an} = \phi_{py}(r_{oav}) + \phi_{ye}(r_{oav}) - n\phi_p, \tag{6.16}$$

but the angle γ_a of the output plane is unaltered.

7. CORRECTION FOR RANGE CURVATURE

7.1 INTRODUCTION

The input range function f in (3.1) is centred in range at

$$r_f = \frac{r_o}{q} + \frac{c_a p^2}{2qr_o}(x_f - x_o/p)^2. \tag{7.1}$$

This quadratically varying offset gives rise to range-curvature aberration. In most radars to date, this aberration has had negligible effect on output image quality. For SEASAT-A, the range-curvature aberration can be sufficiently large to cause image degradation. In this section range curvature is described and methods for correcting it are given.

The effects of range curvature can be described for several locations in the optical correlator. It appears, however, that the region around the Fourier transform plane is best suited for performing the corrections for range curvature. Therefore only this region will be considered here.

In the transform plane distribution G_1, given by (4.1), the range curvature is manifested by the variable f_r in the azimuth focussing factor

$$e^{j \frac{\pi \lambda_r r_o f_x^2}{2c_a p^2 (1+f_r \lambda_r / 2q)}} \tag{7.2}$$

Under conditions well met by SEASAT-A, the azimuth focussing function (7.2) may be approximated as

$$e^{j \frac{\pi \lambda_r r_o f_x^2}{2c_a p^2}} e^{-j \frac{\pi \lambda^2 r_o r f_x^2}{4c_a p^2 q}} \tag{7.3}$$

The first exponential function in (7.3) is just the desired azimuth focussing function in the absence of range curvature. The second exponential function is the error induced by the range curvature. It is possible to construct a lens system [5] or a spatial filter whose transmittance is the complex conjugate to the range-curvature phase function. This device may then be used to cancel the aberration phase factor by matched filtering. However, another approach is taken here, wherein the focussing properties of the exact phase function (7.2) are utilized.

No matter where the effect of range curvature is observed, it is a function of the cross-coupling between the azimuth and range variables. Therefore any correction must always take this cross-coupling into account. In addition, range curvature is a function of r_o and therefore a different correction should be performed for every possible value of r_o. In Section 11.2, it is shown, however, that a single filter can be used over a range of values of r_o to produce an output image of acceptable quality.

7.2 FOCUSSING PROPERTIES IN THE TRANSFORM REGION

Consider now the focussing properties of the transform plane distribution $G_1(f_x, f_r - f_{or})$ given by (4.1). The phase function in f_x^2 represents a focussing in the azimuth dimension. If (7.2) is rearranged and compared to the transmittance (3.11) of a cylindrical lens, then it can be seen that the azimuth focussing function has an equivalent focal length

$$F_{fx} = F_b + \Delta F_{fx}, \tag{7.4}$$

where

$$F_b = \frac{-2p^2 c_a \lambda F_{sl}^2}{r_o \lambda_r} \tag{7.5}$$

and

$$\Delta F_{fx} = \frac{-p^2 c_a F_{sl} r_2}{q r_o}. \tag{7.6}$$

The spatial frequencies (f_x,f_r) have been converted to the distance (x_2,r_2). The "bias" focal length F_b is just the equivalent focal length of the frequency-plane azimuth focussing function in the absence of range curvature and it is a function of r_o. It is wished to maintain this focussing power. The variation ΔF_{fx} in the focal length arises from the range curvature. Notice that it is a *linear* function of r_2. It is also a function of r_o, but over one subswath that variation may be neglected, as will be discussed in Section 11.2.

The azimuth focussing function (7.2) may then be represented as a line source a distance F_{fx} from the transform plane. The linear phase term in f_x in (4.1) causes this line to be shifted in azimuth by a distance proportional to x_o. Thus, for a particular range r_{oo}, point objects at x_{oo},x_{o1}, ... are equivalent to tilted lines in a plane shown in Figure 7.1 where the spacing between lines is proportional to the azimuth spacing of the original point objects. For any other range, r_{on}, there is a similar set of tilted lines located a distance $F_b(r_{on})$ from the transform plane and offset in the range dimension by an amount proportional to r_{on}. The tilt θ_t of all these lines is

$$\theta_t = \tan^{-1}\left[\frac{\Delta F_{fx}}{r_2}\right] = \tan^{-1}\left[\frac{-p^2 c_a F_{s1}}{q r_{oav}}\right] \qquad (7.7)$$

where θ_t is negative as shown in Figure 7.1 and r_{oav} means the average r_o for a subswath.

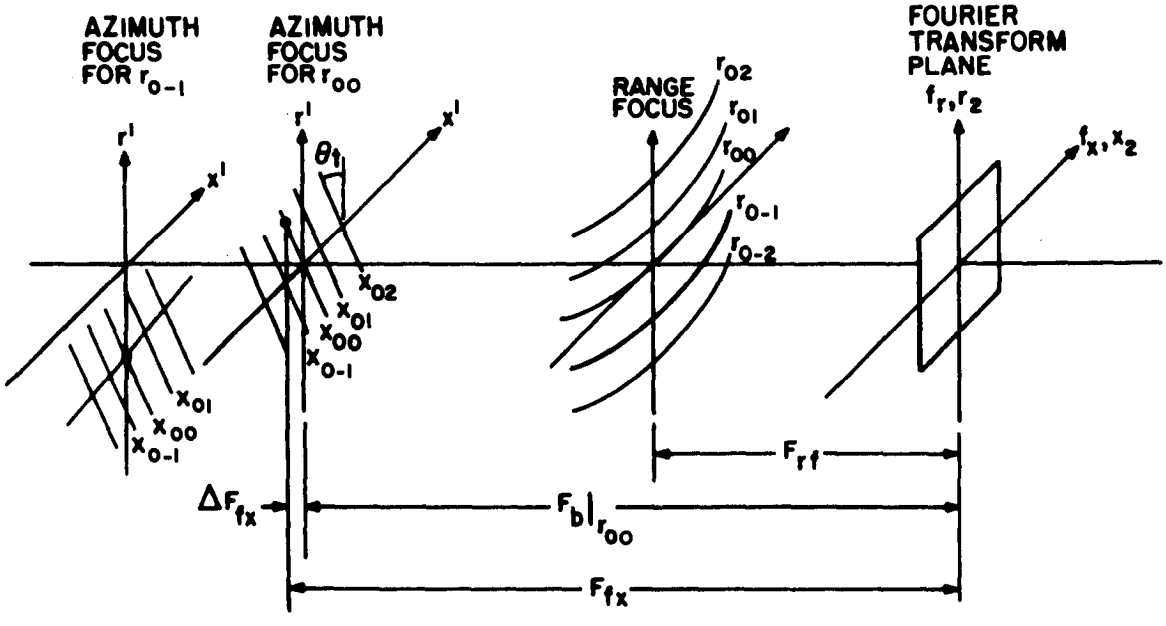

Figure 7.1. Line Focusses of Transform Plane in Range and Azimuth

The term $F(cf_r/2q)$ in (4.1) is the range focussing term. It will have the form of a quadratic phase in f_r^2 if $f(r_f)$ is a linear FM. The equivalent focal length F_{rf}, of $F(f_r)$ is not derived here but can be shown to be independent of x_o and r_o; i.e., it is a constant. The range focussing function may be represented as a line source located a constant distance F_{rf} from the transform plane. The linear phase term in f_r in (4.1) causes this line to be shifted in range by a distance proportional to r_o. Thus, objects at ranges $r_{oo}, r_{o1}, \ldots$, but at any azimuth values x_o, will be imaged at the lines marked $r_{oo}, r_{o1}, \ldots$ in Figure 7.1. As will be discussed later, range curvature causes these lines to be curved quadratically again as shown in Figure 7.1.

In a correlator the interferogram is placed a distance d_i from the transform lens L_{s1}, rather than a distance F_{s1}, so that the amplitude distribution at the transform plane is actually [6]

$$e^{j\frac{\pi}{\lambda F_{s1}}\left[1-\frac{d_i}{F_{s1}}\right](x_2^2+r_2^2)} G_1(f_x, f_r - f_{or})$$

rather than simply G_1 as assumed above. This extra phase function is equivalent to placing a spherical lens of focal length

$$F_d = \frac{-F_{s1}}{1-\frac{d_i}{F_{s1}}} \tag{7.8}$$

at the transform plane. The azimuth focal-length F_{fx} given by (7.4) is thereby modified to be

$$F'_{fx} = \frac{F_{fx}F_d}{F_{fx}+F_d} \tag{7.9}$$

The minimum value of d_i is 0 and its largest practical value would be approximately F_{s1} so that F_d would have a minimum value of $-F_{s1}$ and a maximum of $-\infty$. Since F_d is always fairly large and ΔF_{fx} fairly small, then

$$F'_{fx} \simeq \frac{F_d}{F_b + F_d} F_{fx} \tag{7.10}$$

which is just a constant close to unity times F_{fx}. Therefore the concept of a tilted azimuth line-focus is still valid - its focal length $F_{fx}(r_2)$ is merely scaled by a constant close to unity.

To illustrate the above interpretation of the effects of range-curvature, consider the image planes for a single point-source with range and azimuth such that the various focal lines are centred on the optical axis.

In the absence of range curvature, an erect azimuth-line focus and a straight range-line focus are obtained, as illustrated in Figure 7.2(a). The range focus occurs to the right of the transform plane and the azimuth focus to the left, as will be the case for SEASAT when the input virtual azimuth-image is used.

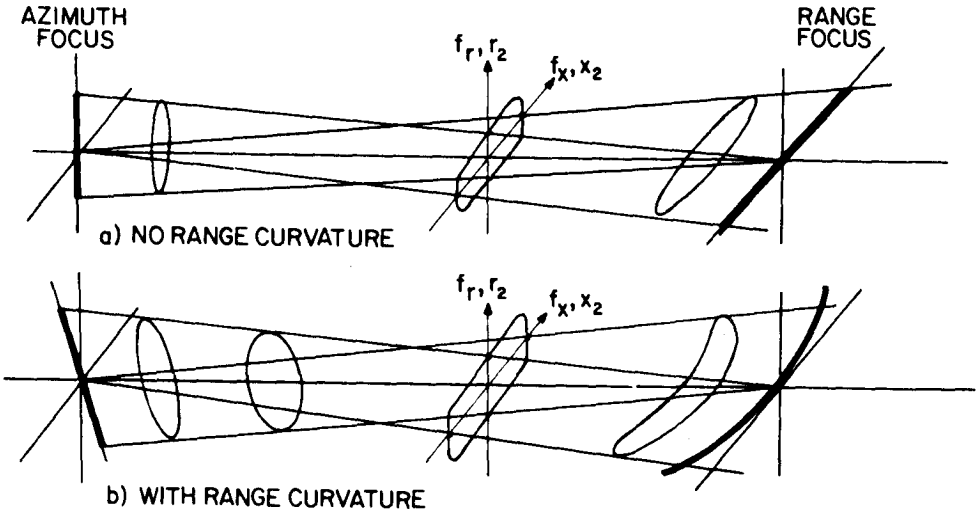

Figure 7.2. Focussing from Azimuth Line through to the Range Focal Line

When range curvature is present, the azimuth image becomes tilted and the range image curved, as illustrated in Figure 7.2(b). That such focussing occurs has been proven separately, by taking eqn. (4.1) describing the transform plane and then solving the propagation equations between the transform plane and the image plane. Note that the interferogram also generates a tilted azimuth and a curved range line-focus. N. Brousseau of DREO has done a detailed analysis of the interferogram focussing properties.

Correction could be done in the region of the interferogram. However the aperture sizes are much larger there than at the transform plane. The line focusses about the transform plane are obviously just the image through lens L_{s1} of the line focusses of the interferogram. Since the azimuth line-focus in the transform region is straight, imaging considerations show that, in the interferogram region, it is curved. However, any curvature is found to have negligible effect for SEASAT-A, and may be neglected.

7.3 TILTED LENS METHODS OF CORRECTION

Numerous points of view and numerous methods of correcting range curvature are possible. Here, the point of view is taken that if the tilt of the azimuth focal line is removed, the degradation of the output image will also be removed. It will be seen in Section 11.3 that range curvature by itself (i.e., when there are no antenna pointing-errors) is relatively small, and therefore approximate methods of correction are sufficient. The effects

of antenna pointing-error can be corrected separately by techniques discussed in Section 7.4.

Two of many possible methods of range-curvature correction are considered here. One merely involves tilting the shift lens. This method appears to be used by ERIM and seems suitable for use on the present DREO correlator. The second method involves the addition of a tilted pair of cylindrical lenses in the region of the transform plane. This method is used by JPL and will likely be used in the new DREO correlator. For both methods a geometrical-optics derivation is used. Although more precise derivations are possible, the approach here is useful for finding approximate values for the tilt and focal length of the corrector lenses. Fine adjustment of the correlator may be made during set-up of the correlator, by observation of the output image.

7.3.1 Tilted Shift Lens

Consider the azimuth shift lens of focal length F_s, located at the Fourier transform plane as shown in Figure 7.3. The tilted azimuth-line is located an average distance F_b', given by (7.5) and (7.10), from the transform plane. The shift lens focusses the tilted azimuth-line to a location an average distance s_o' from the transform plane. Initially it is assumed that rays from each point on the azimuth focal line propagate approximately parallel to the optical axis. For a given value of r_2, it is desired to reposition the lens by a distance Δ from the transform plane, so that the image falls exactly a distance s_o' from the transform plane. The relations between the object-to-lens distance s and lens-to-image distance s' are

$$s = F_b' + r_2 \sin\theta_t - \Delta, \tag{7.11}$$

$$s' = s_o' + \Delta \tag{7.12}$$

and

$$\frac{1}{s} + \frac{1}{s'} = \frac{1}{F_s}. \tag{7.13}$$

Combining (7.11) to (7.13) yields

$$\frac{F_b' + s_o' + r_2 \sin\theta_t}{F_b's_o' + F_b'\Delta + s_o'r_2\sin\theta_t - s_o'\Delta + r_2\Delta\sin\theta_t - \Delta^2} = \frac{1}{F_s}. \tag{7.14}$$

Solution of (7.14) would give Δ as a nonlinear function of r_2. A curved cylindrical lens would be necessary. However, if Δ and $\sin\theta_t$ are small compared to F_b' and s_o', then the last two terms in the deonominator may be neglected and a linear dependence on r_2 is obtained. Thus,

$$\Delta = \frac{-r_2(\sin\theta_t)F_s^2}{F_b'^2 - 2F_b'F_s}. \tag{7.15}$$

Therefore, a lens tilted at an angle

$$\theta_L = \sin^{-1}\left[\frac{-F_s^2}{F_b'(F_b - 2F_s)}\ \sin\theta_t\right] \qquad (7.16)$$

will result in an erect azimuth line-image. Curvature has been neglected by neglecting terms in Δ^2 and $\Delta\sin\theta_t$ in (7.14). For typical values of F_b' and F_s, the value of Δ, and hence θ_L, is found to be very small for SEASAT-A, so that neglecting the curvature is valid. Usually, θ_L will be less than θ_t. Note that θ_L is independent of the image distance s_o', and this distance need not ever be known.

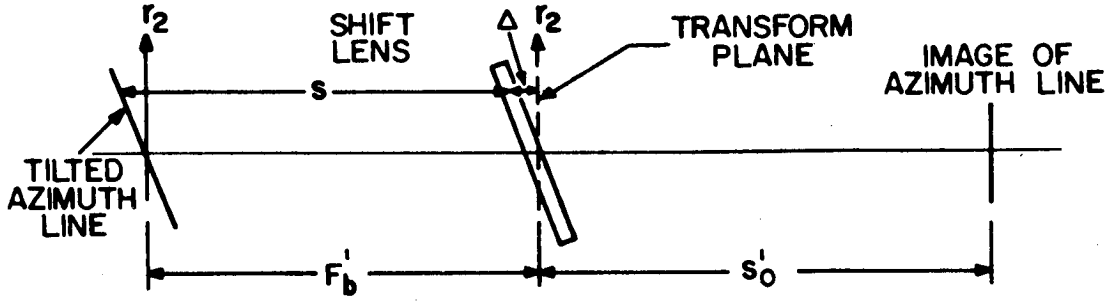

Figure 7.3. Tilted Shift-Lens Method of Range-Curvature Correction

In practice, the rays from the azimuth line are not parallel to the optic axis but converge towards the range focal line. Thus the lens tilt-angle (7.16) will be slightly in error. The simplest approach would be to set the angle approximately according to (7.16), and then adjust it while observing the output image quality.

7.3.2 Additional Tilted-Cylinder Pair

The object here is to add some optical component that makes the azimuth line-focus appear erect when viewed from the transform plane. The range curvature is thereby eliminated. It is further desired that the range line-focus not be shifted or altered. Therefore, cylindrical lenses are indicated. Finally, it is preferable that the azimuth image not be shifted along the optical axis and that the azimuth magnification be unity.

Consider the cylindrical lenses L_1 and L_2 tilted at angles θ_1 and θ_2, as shown in Figure 7.4(a). They are separated by a distance $d_o/2$ along the optical axis, and their centre is a distance d_{on} from the tilted line-focus for range r_{on}. Figure 7.4(b) shows the azimuth cross-section for $r_2 = c_r$, a constant. In an azimuth cross-section, the azimuth line-focus is a distance $s_1(r_2)$ from lens L_1 and its image is a distance $s_2'(r_2)$ from lens L_2. It is desired to have the image S_2' erect. Therefore it is required that $-s_2'(r_2) + r_2\tan\theta_2$ be a constant (s_2' is negative as shown in Figure 7.4). If $F_1 = -F_2$, where F_1 and F_2 are the focal lengths of L_1 and L_2 respectively, then

$$s_2' = \frac{-F_1[F_1 s_1(r_2) + d(r_2)F_1 - d(r_2)s_1(r_2)]}{d(r_2)F_1 - d(r_2)s_1(r_2) + F_1^2} \tag{7.17}$$

where

$$\begin{aligned} d(r_2) &= d_1(r_2) + d_2(r_2) \\ &= d_o - r_2\tan\theta_1 - r_2\tan\theta_2 \end{aligned} \tag{7.18}$$

is the separation between L_1 and L_2 at range r_2. If

$$\theta_1 = \theta_t \tag{7.19}$$

then

$$s_1(r_2) - d_{on} - d_o/2 = s_{o1}, \tag{7.20}$$

which is a constant. Thus

$$-s_2'(r_2) + r_2\tan\theta_2 = \frac{+ F_1[F_1 s_{o1} + d(r_2)(F_1 - s_{o1})]}{d(r_2)\ (F_1 - s_{o1}) - F_1^2} + r_2\tan\theta_2. \tag{7.21}$$

Note in the denominator that $F_1 - s_{o1}$ will be somewhat smaller than F_1 and that $d(r_2)$ can be made small, so that $|d(F_1 - s_{o1})| \ll F_1^2$. It can be seen that neglecting $d(F_1 - s_{o1})$ is the same as neglecting the curvature of the image of the line. If $\theta_1 = \theta_2$, where the positive senses of these angles are as shown in Figure 7.4(a), then

$$-s_2' + r_2\tan\theta_2 \simeq s_{o1} + d_o - d_o\frac{s_{o1}}{F_1} + r_2\left[\frac{2s_{o1}}{F_1} - 1\right]\tan\theta_t. \tag{7.22}$$

Thus the image is shifted a small constant distance $-d_o s_{o1}/F_1$ from the original object, and the tilt has been decreased from θ_t for the object to $\tan^{-1}[(2s_{o1}/F_1 - 1)\tan\theta_t]$ for the image, and is approximately $(2s_{o1}/F_1 - 1)\theta_t$ for θ_t small. If

$$s_{o1} = F_1/2, \tag{7.23}$$

then the image is erect. Since s_{o1} is dependent on range r_{on}, (7.23) is valid only for one range. It will be seen, however, that the variation about the average s_{o1} is small, so that the image is always close to being erect. This is yet another statement that range curvature is not perfectly corrected for all ranges simultaneously. Also note that the azimuth magnification is close to unity, as desired, so that there is no azimuth shift of the output image.

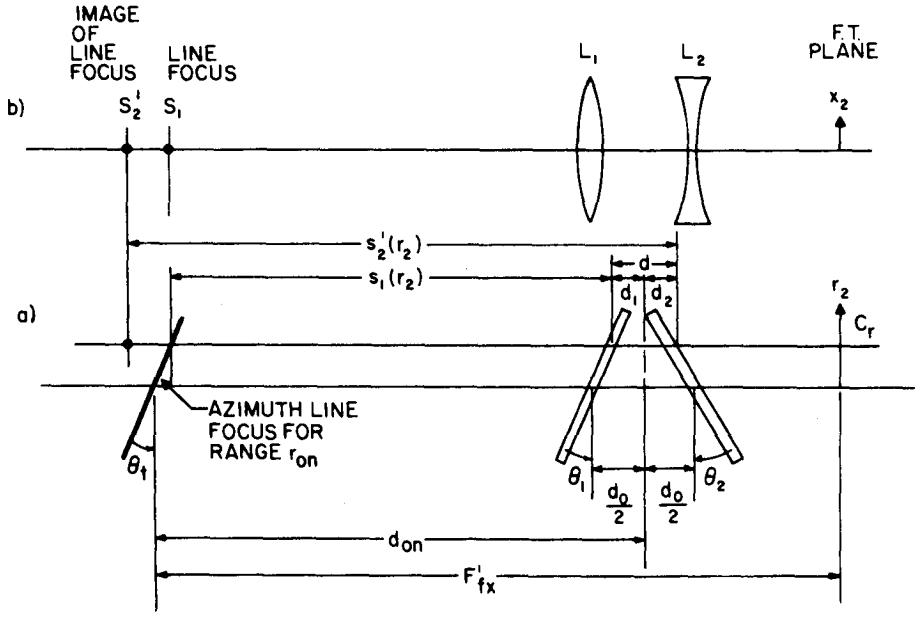

Figure 7.4. Tilted-Lens Range Curvature Corrector with (a) a View through the Plane $x_2=0$ and (b) a View through the Plane $r_2=c_r$

In summary, for a tilted-cylinder pair range-curvature corrector, it is required that:

1) $F_1 = -F_2$,
2) d_o be as small as possible,
3) $\theta_1 = \theta_2 = \theta_t$,

and 4) $s_{o1} \simeq F_1/2$.

7.4 CORRECTION IN THE PRESENCE OF ANTENNA POINTING ERROR

In Section 6, it was seen that practical considerations dictate that the light beam should be steered to correct for antenna pointing errors (pitch, yaw and equivalent yaw). The envelope of the spectrum is thereby centred on the optical axis. Unfortunately, the phase functions are equally shifted. The effect of shifting the azimuth focussing phase function, the first factor in (7.3), has been described in Section 6.1 and is summarized in Table 6.1. The range curvature function, the second exponential factor in (7.3), becomes, after shifting

$$e^{\frac{-j\,\pi\lambda^2 r_o f_r (f_x - f_s)^2}{4c_a p^2 q}} = e^{\frac{-j\pi\lambda^2 r_o f_r f_x^2}{4c_a p^2 q}} \; e^{\frac{j\pi\lambda^2 r_o f_r f_x s}{2c_a p^2 q}} \; . \; e^{\frac{-j\pi\lambda^2 r_o f_r f^2 s}{4c_a p^2 q}} \qquad (7.24)$$

where f_s is the azimuth-frequency offset caused by tilting the illumination beam and is given by

$$f_s = f_{apy} + f_{aye},$$

$$= \frac{2c_a p}{\lambda_r r_{oav}} (x_{pya} + x_{yea}). \tag{7.25}$$

It is possible to correct fully the shifted range-curvature function (7.24) merely by taking the correctors described previously and shifting them in azimuth by $\lambda F_{s1} f_s$; i.e., by the same shift as for the envelope of the spectrum. However, for the large values of f_s experienced by SEASAT-A, corrector lenses with very large apertures are needed. Aberration correction over such large apertures could be difficult.

Another approach is to expand the shifted range-curvature function into the three phase factors given on the right-hand side of (7.24) and then deal with the three aberration terms individually. This approach appears to be taken at both JPL and ERIM. The first factor is just the unshifted range-curvature factor considered previously. Therefore, techniques such as those described in Section 7.3 can be used for the correction. No shifting of the corrector is needed as antenna pointing error changes.

The third factor is a linear phase shift in f_r. Therefore its only effect on the output image of a point is to shift the image by the amount

$$\Delta r_4 = \frac{\lambda^2 r_o f_s^2}{8c_a q p^2} \tag{7.26}$$

where r_2 is the range dimension in the output plane. In most applications, such an offset is acceptable, since it is known at least as accurately as the offset f_s is known. As f_s changes with latitude, the range reference-line calibration would have to be altered. Since the offset is dependent on r_o, there will be some distortion. However, processing will be done over only a quarter-swath of extent $\Delta r_o \simeq 9$ km, whereas the total range r_o is $\simeq$850 km. Thus, the distortion is small, $\simeq$0.5%. Therefore, this aberration factor will usually be neglected.

The second factor in (7.24) is a cross coupling between f_x and f_r. It seems to be referred to at JPL and ERIM as the range-walk factor. However, range walk is most commonly related to a radial motion of the target during the recording interval, whereas for SEASAT-A this factor is an effect arising from an antenna pointing-error. Therefore, the term "range walk" appears inappropriate. For lack of a better name, the second factor will be referred to here as the linear cross-coupling function. A simple method of eliminating this factor is discussed below.

The second factor in (7.24) may be rewritten in terms of the spatial coordinate of the transform plane as

$$e^{\frac{j\pi\lambda_r x_2 r_2}{pqF_{s1}^2\lambda^2}(x_{pya} + x_{yea})}. \tag{7.27}$$

The transmittance of the azimuth shift-lens as shown in Figure 7.5(a) is

$$e^{\frac{-j\pi x_2^2}{\lambda F_{as}}} \tag{7.28}$$

where F_{as} is the focal length. Upon rotation about the optical axis by an angle ϕ, its transmittance becomes

$$e^{\frac{-j\pi x_2'^2}{\lambda F_{as}}} = e^{-\frac{j\pi}{\lambda F_{as}} x_2^2\cos^2\phi} \; e^{-\frac{j\pi}{\lambda F_{as}} 2\cos\phi\sin\phi x_2 r_2} \; e^{-\frac{j\pi}{\lambda F_{as}} \sin^2\phi r_2^2} \tag{7.29}$$

The first phase factor in (7.29) is almost the same as that for the unrotated shift lens in (7.28), except that the focal length is now $F'_{as} = F_{as}/\cos^2\phi$, which for ϕ small is close to F_{as}. A slight azimuth refocussing of the correlator may be necessary. The third factor is a range shift-lens with focal length $F_{as}/\sin^2\phi$, which is very large for ϕ small. This lens may therefore have negligible power.

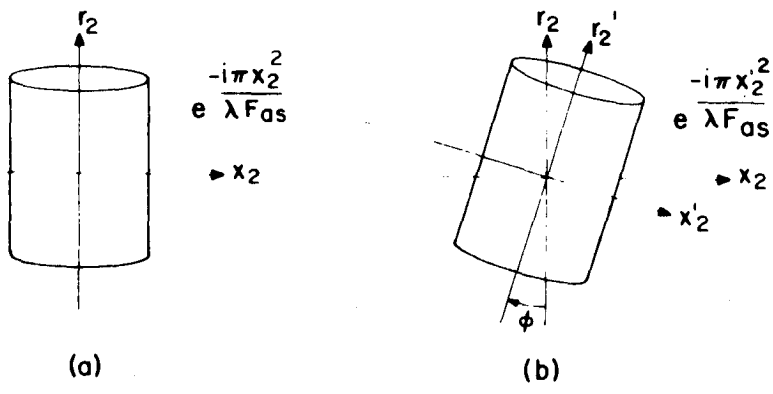

Figure 7.5. Azimuth Shift Lens in (a) Normal Position and (b) after Rotation to Correct for the Linear Cross-Coupling Aberration

The second phase factor can be chosen to cancel the linear cross-coupling aberration (7.27). There is exact cancellation when ϕ is chosen such that

$$\cos\phi \sin\phi = \frac{-\lambda_r F_{as}}{2pq F_{sl}^2} (x_{pya} + x_{yea}) \tag{7.30}$$

For ϕ small, $\cos\phi \sin\phi \simeq \phi$. For F_{sl} = 570 mm, $x_{pya}+x_{yea}$ = 20.2 km (maximum at Shoe Cove), previously listed values of λ, p, q and λ_r, and, as an example, F_{as} = 73 mm, it turns out that $\phi = 0.93°$. This value is quite small. Note that ϕ is independent of range r_o.

Thus, a simple method of cancelling the linear cross-coupling function is possible. It can be combined easily with any of the methods for correcting the range-curvature factor. It is particularly straightforward when range curvature is corrected by the method of tilting the shift lens - no additional optics are needed for any of the corrections. The rotation ϕ can be calculated from (7.30) from the values of $x_{pya}+x_{yea}$ used. In practice, it may be simpler to observe the output image while adjusting the angle ϕ to give the best image.

7.5 PARAMETERS FOR THE TILTED AZIMUTH FOCAL LINES

In Table 7.1, some parameters for the tilted azimuth focal-lines are given. The values F_{sl} = 570 mm and λ = 632.8 nm were used in all the calculations. The bias focal length F_b given by (7.5) varies with r_o and is given only for the average value of r_s of each subswath. The values for F_{fx} rather than F'_{fx} are given because the value of distance d_i has not yet been determined. Since the scaling given by (7.10) between F'_{fx} and F_{fx} is close to unity, the values of F_{fx} are close to the values of F'_{fx} anyway. The maximum value of ΔF_{fx} was calculated from (7.6) using the maximum value of r_2 which, from Table 4.1, is ±6.1 mm. The value of θ_t was calculated from (7.7). The tilt angle θ_t is relatively small. Recall that the tilt angles of the cylindrical-pair range-curvature corrector lenses are $\theta_1 = \theta_2 = \theta_t$. As an example, let the focal length of the azimuth shift lens be 73 mm. Then for the tilted shift-lens method of curvature correction, the tilt is calculated from (7.16) to be $\theta_L \simeq 4.0°$, the same as θ_t. Usually θ_L will be less than θ_t.

TABLE 7.1

Parameters of the Tilted Azimuth Focal Lines

Subswath Number	r_{sav} km	F_b mm	$\Delta F_{fx\|max}$ mm	θ_t
1	840.16	-67.2	∓0.44	-4.1°
2	849.76	-66.5	∓0.43	-4.1°
3	859.36	-65.7	∓0.43	-4.0°
4	868.96	-65.1	∓0.42	-4.0°

8. DOPPLER-CENTROID ESTIMATION

In Section 6 it was assumed that a knowledge of pitch, yaw and equivalent yaw was available, so that the steering mirror could be rotated appropriately to compensate. In particular, it was to be rotated in proportion to $x_{pya}+x_{yea}$, the pitch and yaw for the average range, r_{oav}. Typical values of x_{ye} and maximum values of x_{py} are given in Table 3.4. To determine $x_{pya}+x_{yea}$ optically, it is proposed to utilize the observed spectrum itself. The

intensity of the spectrum in the f_x dimension is proportional to $|h''(f_x+f_{xpy}+f_{xye})|^2$, where h'' is a form of the amplitude h of the two-way antenna pattern with multiplicative constants absorbed. The objective is to estimate $f_{xpy}+f_{xye}$ from measurements on $|h''|^2$. Several estimators, such as detecting the peak of $|h''|^2$ or calculating the centroid of $|h''|^2$, could be used. From a knowledge of $f_{xpy}+f_{xye}$ at the average range r_o, $x_{pya}+x_{yea}$ is calculated from (4.7). Unfortunately, a number of problems arise that make centroid estimation difficult. These problems are discussed below, followed by a discussion of where and how the centroid should be measured.

8.1 SEPARATION OF THE SPECTRAL ORDERS

The first problem is how to distinguish between the repeated spectra. As illustrated in Figure 4.1, spectra are repeated in azimuth frequency at intervals of 1 PRF. Measurement of $f_{xpy}+f_{xye}$ must be made on only one of these spectra. As the PRF (f_p or f_{xp}) approaches the value of the bandwidth (Δf_d or B_x), the valleys between the peaks become shallow. It may be difficult to distinguish a peak from a valley, making it difficult to measure the doppler centroid. It is estimated by JPL that the peak-to-valley ratio is 8.3 dB at the highest PRF and 6 dB at the lowest. Effects of noise and target distribution statistics could reduce this ratio. Furthermore, measurement in the (f_x,f_r) plane decreases the ratio for reasons to be described below.

The separation between spectra is now considered. In Section 4, a two-way 3-dB doppler bandwidth of Δf_d = 1040 Hz (B_x = 26.0 c/mm) was assumed. The maximum PRF of f_p = 1647 Hz (f_{xp} = 41.2 c/mm) will likely be used most of the time. Thus a gap of 607 Hz (15.2 c/mm) is expected between the 3-dB points. For the (f_x,f_r) plane, as shown in Figure 4.1, this gap is applicable only to objects at a single range. From (3.4), (3.5) and (4.7), it is seen that the doppler centroid $f_{xpy}+f_{xye}$ is range dependent. For example, at the latitude of Shoe Cove (ϕ_o = 52.5°) and for minimum and maximum slant ranges of 835.4 km and 873.8 km respectively, the worst-case shifts of the spectra are as shown in Table 8.1. Thus the gap between spectra is reduced by 316 Hz (7.9 c/mm) to 291 Hz (7.3 c/mm) as illustrated in Figure 8.1. This reduction in the gap is for the entire swath width whereas normally only the spectrum for a quarter swath would be used, so that the gap would be narrowed only by approximately 316/4 Hz.

TABLE 8.1

Frequency Offsets for Minimum and Maximum Range at ϕ_o = 52.5° (Shoe Cove)

	r_o = 835.4 km	r_o = 873.8 km	Column 1 −Column 2
$f_{py}+f_{ye}$ Hz	1507	1823	316
$f_{xpy}+f_{xye}$ c/mm	37.7	45.6	7.9

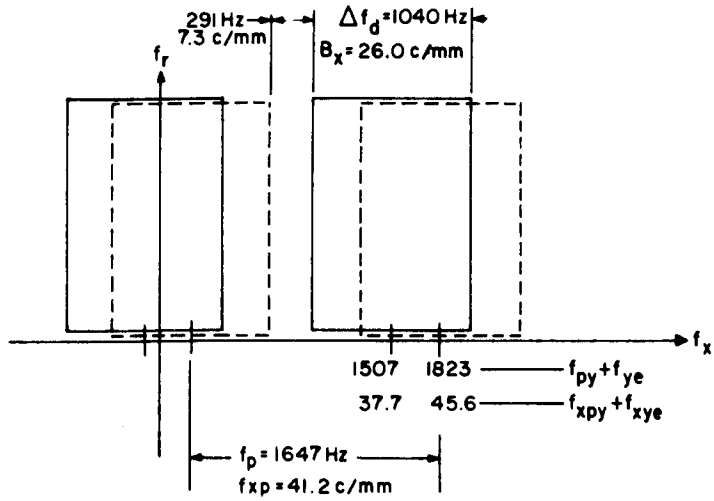

Figure 8.1. Two-dimensional spectrum showing 0 and -1 orders only. For each order the region of the spectrum for both minimum and maximum range are given.

If the narrowing of the gap causes the peak-to-valley ratio to decrease excessively, it is possible to eliminate this problem by using a one-dimensional spectrum. One dimension is still azimuth frequency f_x, but in the other dimension, r_4, the input signals has been compressed (focussed) to a range image. By this manoeuvre, the spectra for each range are separated by the full gap as illustrated in Figure 8.2.

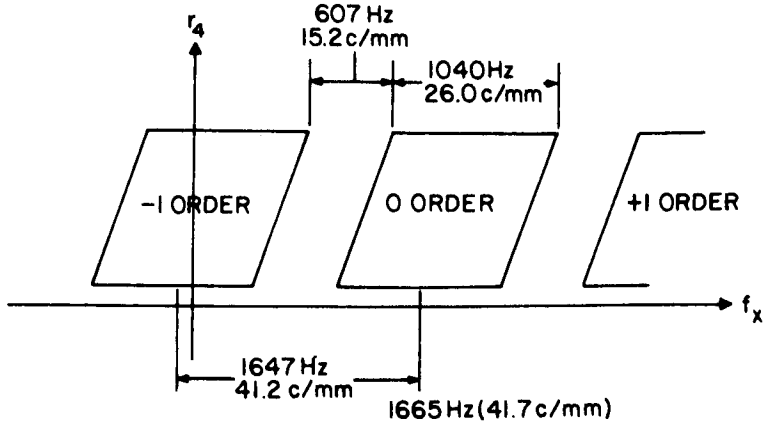

Figure 8.2. The One-Dimensional Spectrum as a Function of f_x, r_4 for a Full Swath

8.2 IDENTIFICATION OF THE SPECTRAL ORDER

The second problem that arises is the one of ambiguity. It is necessary to know which spectral order is being used in the determination of $f_{xpy}+f_{xye}$. Each order is usually distinguished only by its position relative to $f_x=0$. However, pitch, yaw and equivalent yaw can cause the spectra to shift. Since the offsets given in Table 4.2 can be greater than 1/2 of the maximum separation f_{xp}, the selection of the desired spectral order becomes ambiguous. From orbital data it should be possible to calculate x_{yea} accurately from (3.5) and thence f_{xye}. However, f_{py} or f_{xpy} alone can be up to 1/2 of f_p or f_{xp}, leaving some danger of ambiguity. In this case the ambiguity can be reduced to knowing that the correct spectrum is one of only three spectra. In principle, the correct spectrum can be located by forming separate images for each of the 3 possible candidates and comparing the three images. The two incorrect spectra will give defocussed and distorted images. However, it may not generally be obvious which images are distorted or defocussed, especially when looking at ocean surface. At JPL the ambiguity will be resolved by the use of independent attitude data, available post-pass from NASA. These data give θ_y and θ_p to an accuracy of $\pm 0.2°$ to the 3-σ points. Since the maximum offset of f_{xpy} is approximately 1/2 of f_{xp} and is based on a maximum error in θ_p and θ_y of $\pm 0.5°$, then a calibration of θ_p and θ_y to $\pm 0.2°$ will establish f_{xpy} to less than 1/4 of f_{xp}. Thus ambiguities are eliminated. Once the correct spectrum is located, then the centroid estimator may be locked to this spectrum for the remainder of the pass, thus eliminating further concern about ambiguities. Note also that the ambiguity needs to be resolved not only for doppler-centroid estimation, but also for selection of the correct order for the correlator itself.

8.3 THE EFFECT OF SPECTRAL AMPLITUDE WEIGHTING

The third problem is the one of the heavy spectral weighting shown in Figures 4.2 and 4.3. This problem arises only in optical processors, because of the non-zero line width recorded on the interferogram. Several difficulties arise because of this weighting. First, as seen in Figure 4.3, the various spectra become asymmetric, which means that neither the peak nor the centroid corresponds to the desired value $f_{xpy}+f_{xye}$. Second, the peak-to-valley ratio will be altered, likely in a detrimental manner. Third, only at the most two spectral orders will have significant magnitude. It will therefore be necessary to perform the centroid measurement on the most intense spectrum, not necessarily the zero-order spectrum. Therefore some method of switching the detector from one spectral-order to another should be incorporated. Upon switching, care must be taken to account for the effect of this switch upon the calculation of $f_{xpy}+f_{xye}$.

8.4 TECHNIQUES FOR OBSERVING THE AZIMUTH-FREQUENCY SPECTRUM

As mentioned previously, the value of the centre frequency may be measured either at an azimuth-frequency, range-frequency (f_x,f_r) plane or at an azimuth-frequency, range-image plane. In the tilted-plane processor, the two-dimensional frequency (f_x,f_r) plane is just the focal plane of the lens L_{s1}. If it is desired to perform Doppler-centroid estimation simultaneously with the correlation operation, a beam splitter could be used to split off a portion of the light power from the order being utilized for image formation.

This method is undesirable, because of the loss of light power and because of the potential for degrading the output image. However, since only one of the two orders of range spectrum is utilized in image formation, the unused range spectral order could be used instead, as JPL is going to do. The disadvantage of using this spectrum is that lens L_{s1} must be capable of handling the wider spatial-frequency bandwidth. The lens used by JPL will be able to do this. It appears that if the interferogram and lens L_{s1} are reasonably close together, the DREO lens L_{s1} should also be adequate for producing a usable spectrum.

A substantial advantage arises in the above techniques in that, since the tilting of the input illumination corrects for pitch, yaw and equivalent yaw, the spectrum will always be nearly centred. Therefore neither the aperture stop needed to block all but the desired spectral order, nor the device used for measuring $f_{xpy}+f_{xye}$, need to be tracked relative to the centre of the spectra. They will be stationary even when there is a switch between spectra. The centroid-estimation device will measure the error $\Delta[f_{xpy}+f_{xye}]$ in the shift of $|h''|^2$ rather than the absolute shift $f_{xpy}+f_{xye}$, and then use this information to adjust the tilt of the input illumination mirror. Because this is a classical feedback system, some care must be taken to ensure its stability.

Two other methods of obtaining the two-dimensional spectrum are noted. I. Henderson of DREO has suggested using the unused section of interferogram that extends outside the input-aperture region (since the DREO films will cover two subswaths) with a separate laser source for illumination. Care would be necessary in relating the frequency offset measured at one range to the actual offset at another. As a second method, a separate laser beam could be used to illuminate the input aperture. This laser beam could perhaps be narrow compared to the main illumination beam, and could possibly be inclined sufficiently so as to bypass lens L_{s1}.

If the centroid estimation is performed simultaneously with the correlation, as it was assumed above, this causes certain practical difficulties. A recommended alternative is to perform the estimation on a separate initial run. Then the full main beam of the correlator can be utilized, and the centroid estimator can be placed directly at the main Fourier-transform plane. (The shift lens and range-curvature lenses would be removed.) The feedback system to control the tilting mirror would likely still be utilized. The tilt of the mirror as a function of satellite position would be recorded and then used appropriately during correlation.

To obtain an azimuth-frequency, range-image (f_x,r_4) plane, it is necessary to add certain cylindrical optics. Only if the overlap problem illustrated in Figure 8.1 becomes serious would it be worth the effort of adding these extra optics.

8.5 OPTICAL METHODS FOR ESTIMATING THE DOPPLER CENTROID

Optical methods for estimating the Doppler centroid from the (f_x,f_r) or (f_x,r_4) plane distribution will now be considered. JPL is proposing to use a linear-position-sensing device of the LSC series made by United Detector Technology Inc.. As far as can be interpreted from its data sheets, it appears that the device with its associated amplifier gives an output, V, proportional to the centroid of the light falling on the detector surface, such that

$$V = c_5 \int_{-a/2}^{a/2} f_x \left| h''(f_x+f_{xpy}+f_{xye}) \right|^2 \, df_x \qquad (8.1)$$

where c_5 is a constant and a is the width of the aperture stop.

There are several difficulties in using the centroid to estimate $f_{apy}+f_{aye}$. First, it is assumed that $|h''|^2$ is symmetric whereas, as seen in Figure 4.3, it is asymmetric because of the amplitude-weighting function. Thus, errors will occur. Second, the spectra for many ranges are superimposed, along with the one for r_{oav}. Therefore the centroid gives some sort of average $f_{xpy}+f_{xye}$, not necessarily the desired $f_{apy}+f_{aye}$. Third, in the presence of repeated spectra, the centroid-estimation method could well fail because of overlapping between spectral orders. Preliminary results from a Queen's University study contract indicate that centroid estimation will not give reliable values of $f_{apy}+f_{aye}$, whereas peak detection will. Obviously an aperture stop is necessary to block all other of the repeated spectra. Even so, any shift of the spectra will bring parts of adjacent spectra within the aperture, thereby upsetting the centroid estimation.

A more appealing approach is to use peak detection. Linear arrays of photodiodes are readily available and multichannel optical-analyzers (at least one of which has been in use at CRC for several years) come with computing power built in. If $|h''|^2$ is symmetric, the peak occurs at $f_x = -f_{xpy}-f_{xye}$. When the weighting of Figure 4.3 makes h" asymmetric but the weighting is well known, it is possible to derive a correction table that relates the measured position of the spectral peak to the value of $f_{xpy}+f_{xye}$. The computing ability of the analyzer could also be used to smooth the detected spectrum to improve the estimate of the peak position. In practice it may be more appropriate to detect a valley rather than the peak.

It is estimated at JPL that the centroid can be estimated to an accuracy of about 10%. Therefore it is their intention to allow the spectrum to drift by up to 10% before making any change in correction by tilting mirrors, etc.. Thus all motions of the mirrors and the shift lens will occur in discrete steps.

For any method of measurement of $f_{xpy}+f_{xye}$, it may be necessary to perform time averaging to reduce the effects of noise and other problems. At JPL the centroid estimation will be averaged over 10 seconds. Presumably, in 10 s the pitch and yaw of the satellite remain sufficiently constant to take a valid average.

9. MULTIPLE LOOKS

SAR images of diffuse extended objects can have a granular appearance, sometimes called speckle, arising from the fact that the microwave illumination is coherent. Image quality can be improved either by improving resolution by means of increased coherent integration (i.e., by using longer correlation apertures) or by improving the signal-to-noise ratio by means of incoherent

averaging of independent images. Incoherent averaging is obtained at the sacrifice of resolution. A debate continues as to what combination of coherent and incoherent integration leads to the best image interpretability. In the SAR literature incoherent averaging is also referred to as mixed-integration or multiple-look processing.

For SEASAT-A, division of the azimuth beam into up to 4 "looks" is being considered. As seen in Table 3.5, utilization of the full azimuth beam leads to an input aperture of 80.5 mm and an azimuth resolution of 6.5 m. However the resolution objective is only 25 m, for which an aperture of only 20.7 mm is needed. The 80.5 mm full-resolution aperture may therefore be divided into 4 slightly overlapping subapertures of 20.7 mm. If the 4 looks are processed separately and the resulting 4 images incoherently averaged, a gain in signal-to-noise ratio of slightly less than 2 times (3-dB) may be expected. Since the loss in resolution is 25/6.5 = 3.8 times, the wisdom of such an operation may be questioned. It appears that at JPL, full azimuth resolution (6.5 m) imagery will be produced except if a user specifically requests reduced resolution (25 m).

It can be argued that things such as ionospheric effects may sometimes make it impossible to focus (coherently integrate) correctly over an entire full aperture. Such occurrences will likely have an inherent incoherent averaging effect causing a degradation of the resolution towards the 25 m value. Thus the overall effect ought to be similar to that obtained by multiple-look processing.

Incoherent averaging in azimuth can be implemented on an optical correlator in numerous ways. First, it is possible to divide directly the input aperture into looks by placing a 20.7 mm azimuth stop (for r_{oav}) at the interferogram plane. In a tracking correlator such as the tilted-plane processor, both the input and output film may be in constant motion. If so, all looks will be imaged simultaneously across the azimuth output aperture, and will be recorded on the output film. All the looks will be properly superimposed in a continuous multiple exposure, which is the same as incoherent averaging. A serious disadvantage to this method is that the output azimuth aperture must be as wide as a full synthetic aperture. Normally the output aperture is kept small, of the order of 50 to 100 resolution elements. To make it both large and free of aberrations is a difficult task.

The second method of incoherent averaging involves reducing the width of the aperture stop at the transform plane. For β = 16 mRad, an aperture stop of width B_x = 26.0 c/mm was calculated from (4.3). In Section 3.2, it is seen that for 25 m resolution a beam width of only 4.2 mRad is needed, which, from (4.3), means that $\Delta f_d' = 2 \times 7.64 \times 10^3 \times 0.0042/0.235 = 273$ Hz and an aperture stop of only $B_x' = 273/40 = 6.8$ c/mm is required. If this aperture is kept stationary, a output of 25 m resolution is obtained, but it has no incoherent averaging, i.e., it is a single look at 25 m resolution. However, if this subaperture is rapidly scanned past the main aperture of width B_x = 26.0 c/mm, then multiple exposures of the image will be made on the film, which corresponds to incoherent averaging. A slit in a rotating disc is the simple method of implementing such a scanning aperture.

The third method of incoherent averaging involves forming a full resolution image and then smoothing it in such a manner as to give incoherent

averaging. It appears that this method will be used at JPL. They are using the simple approach of slightly mismatching the output recording film velocity v_r to the input interferogram film velocity v_i. As will be seen in Section 10, the velocities are normally chosen so that

$$\frac{v_r}{v_i} = A_o \tag{9.1}$$

where A_o is the azimuth magnification of the correlator (here $A_o < 1$). With this ratio, perfect tracking occurs and a full resolution image is obtained. If the recording film velocity is now altered to be $v_r' = v_r + \Delta v_r$, then the tracking is upset. Suppose an aperture stop of width w_x is placed against the recording film. Let the point on the film centered in the aperture be the reference for which we say the image falling on the film is correctly located. At another instant, the moving image will not fall exactly on this same point because of the mismatch in tracking. At the edge of the aperture, a distance $\pm w_x/2$ from the center, let the displacement or tracking error be $\pm\rho_{Ra}A_o/2p$ where $\rho_{Ra}A_o/p$ is the desired resolution as measured at the output plane. For $\rho_{Ra} = 25$ m, $p = 169{,}027$ and $A_o \simeq 0.2$ (see Table 5.1) $\rho_{Ra}A_o/p = 30$ μm. By this process, the resolution recorded on the film is reduced to 25 m from 6.5 m but the image has been incoherently integrated appropriately. The velocity offset required is

$$\Delta v_r = \frac{v_r \rho_{Ra} A_o}{p w_x} . \tag{9.2}$$

Note that the velocity offset is dependent on the aperture width w_x. If $w_x = 1$ mm, $v_r = 1.0$ mm/s and $\rho_{Ra}A_o/p = 0.03$ mm then $\Delta v_r = 0.03$ mm/s which is an offset of 3%. It perhaps has not escaped the reader's notice that, by recording on film whose resolution is about 30 μm, a smoothing of the microwave speckle will also occur.

Notice that, in methods two and three, rather than having 4 discrete looks, the looks are continuously scanned. By such scanning it may be shown [7] that, for a rect window, the SNR of the image is increased by about $\sqrt{3/2}$ (0.9 dB) and by almost 2 dB for a cosine (Hanning) window.

Finally, note that microwave speckle is to be distinguished from the laser speckle that arises in coherent optical processors. Laser speckle is reduced without loss of resolution by use of a tracking system (see Section 10).

10. OUTPUT PARAMETERS

10.1 GENERAL

In this section, some of the parameters of the output plane are discussed, and these parameters are summarized in Table 10.1. The output plane, P_4, as shown in Figure 5.1, has azimuth and range coordinates x_4 and r_4 respectively. It is tilted by angle $\alpha' = \alpha$ where α is given for each subswath in Table 5.1. If unity range magnification is used, the range aperture for one subswath is seen, from Table 3.5, to be 47.9 mm.

TABLE 10.1

Some Parameters of the Output Plane

tilt angle $\alpha' = \alpha$	See Table 5.1
range aperture for one subswath	47.9 mm
azimuth aperture, w_x	
a) "snap-shot" mode	$\simeq$ 50 mm
b) normal tracking	$\simeq$ 1 mm
c) mismatched tracking	see equation (9.2)
range -3 dB point-image size	23 μm
ground-range resolution	
a) -3 dB	19m
b) Rayleigh	21m
azimuth -3 dB point-image size Δx_4	
a) 25 m resolution	30 μm
b) 6.5 m resolution	7.7 μm
recording film should have MTF good to at least	
a) for $\Delta r_x \rightleftharpoons 23\mu$m ($\rho_{3rg}$ = 19 m)	19 lp/mm
b) for Δx_4 = 30 m (ρ_{Ra} = 25 m)	15 lp/mm
c) for Δx_4 = 7.7 m (ρ_{Ra} = 6.5 m)	57 lp/mm
scale factor	1:817,000
magnification of relay lens to give scale of 1:500,000*	1.63X
Film Drive	
v_r/v_i	$A_o \simeq 0.2$ (see Table 5.1)
v_r	to be decided, possibly 1 mm/s
permissible constant error in velocity ratio if w_x = 1 mm	
a) for 25 m resolution	0.7%
b) for 6.5 m resolution	0.2%
maximum instantaneous positional error (jitter)	
a) interferogram	37 μm
b) recording film	7 μm
flutter at 0.5 Hz	<1.2%
10.0 Hz	<23%
film type and size	to be decided

* *If a relay lens is used, all the apertures listed in this Table are increased by 1.63X, the spatial frequencies are reduced by 1.63X and the velocity ratios are altered appropriately.*

The choice of azimuth-aperture width w_x depends upon by which of the two modes the image is recorded. For the "snap-shot" mode, the input and output films are stationary and a wide output aperture is necessary. To date, all imagery at DREO has been produced this way. If it is desired to record a continuous strip map and, simultaneously, to reduce laser speckle, the tracking capability of the tilted-plane processor can be utilized. Note that the methods of reducing microwave speckle discussed in Section 9 will simulaneously reduce the laser speckle.

Usually a relatively narrow output-aperture slit is associated with tracking operation. Such a narrow slit eliminates wide-angle aberrations and thereby reduces design problems for the azimuth telescope. For normal tracking, the exact width w_x is not too critical - perhaps of the order of 30 resolution elements. As seen in Section 9, a resolution element has a width

$$\Delta x_4 = \frac{\rho_{Ra} A_o}{p} \tag{10.1}$$

which, for ρ_{Ra} = 25 m and $A_o \simeq 0.2$ (see Table 5.1), implies that $\Delta x_4 \simeq 30$ μm. For ρ_{Ra} = 6.5 m, $\Delta x_4 \simeq 7.7$ μm. An aperture $w_x \simeq 30 \times 0.03$ mm $\simeq 1$ mm appears reasonable. If microwave speckle is to be reduced by means of the mismatched tracking method, then the aperture width w_x is much more critical and must be chosen according to (9.2).

In azimuth, a point image has a nominal intensity distribution of $\text{sinc}^2(x_4/\Delta x_4)$ if rect weighting is used. This distribution will not normally be achieved in practice. For illustration purposes, suppose that the point image has an approximately Gaussian intensity distribution of width Δx_4 at the 1/2 intensity points. Such a point image has a spatial frequency (f_4) distribution $\exp[-(1.89\Delta x_4 f_4)^2]$. This frequency distribution falls to 1/2 at $f_4 = 0.44/\Delta x_4$. Therefore, the recording film should have a MTF good to at least f_4 = 15 lp/mm for Δx_4 = 30 μm and to at least f_4 = 57 lp/mm for Δx_4 = 7.7 μm.

In range, a point image has a nominal intensity distribution of $\text{sinc}^2(2qB_2 r_4/c)$. For q = 306,000 and B_2 = 19 MHz, the 1/2 intensity width is $0.886c/(2qB_2)$ = 22.9 μm. The dimension r_4 represents ground range r_g with a scaling

$$\Delta r_g = q\, M_{rc}\, \Delta r_4 \tag{10.2}$$

where M_{rc} is tabulated in Table 3.3. For subswath 2, a width of 22.9 μm is therefore equivalent to a ground-range resolution of ρ_{3rg} = 306,000 x 2.67 x 22.9 x 10^{-6} = 18.7 m or a Rayleigh resolution of ρ_{Rrg} = 21.1 m.

The object-to-image scale should be the same in azimuth and in ground range, in order to achieve the desired unity aspect ratio. In azimuth, the object-to-image scale is

$$\frac{x}{x_4} = \frac{p}{A_o}. \tag{10.3}$$

Consider subswath 2 for which $A_o = 0.207$; then $x/x_4 = 817000$. The ground-range scale is found from (10.2) to be $r_g/r_4 = q\, M_{rc}$. For subswath 2, $M_{rc} = 2.670$ so that $r_g/r_4 = 817000$ also. If an even scale factor of 1:500,000 is desired, then a magnification of 1.63X is required. It may be performed by the addition of a relay lens, properly tilted and adjusted to give the 1.63X magnification. Alternatively, the image may be recorded on film at the 1:817000 scale and subsequently be enlarged.

10.2 FILM DRIVE STABILITY

When the correlator is operating in the tracking mode, the input interferogram film velocity v_i and the recording velocity v_r must be chosen so that they have exactly the ratio

$$v_r/v_i = A_o. \tag{10.4}$$

where A_o is the azimuth magnification of the optical system. The velocity v_i must also be selected so as to give the best combination of exposure and throughput. The accuracy and stability required for the two film drives will be discussed below. Note that the difference in stability requirements between recording the interferogram [1] and recording the image is similar to that between recording and reconstructing a hologram. In general, the stability requirements for constructing the interferogram (hologram) are much stricter than for reconstructing the image. Thus, it should not come as a surprise that the film drive requirements which follow are not as strict as for the recorder [1].

Consider first the problem of a constant error in the velocity ratio. the error can come from inaccurate setting of v_i or v_r, from inaccurate measurement of A_o, or any combination. Since the absolute values of v_i and v_r are not important, but their ratio is, let the entire error be assigned to the ratio A_o. Thus, the actual velocities v_i' and v_r' have a ratio

$$v_r'/v_i' = A_o + \varepsilon \tag{10.5}$$

and the error ε can arise from errors in setting v_i or v_r, or in measuring A_o. One effect of the error is to alter the azimuth scale factor of the output image from A_o/p to $(A_o + \varepsilon)/p$. Thus, ε is first specified to give the desired scale accuracy. A more serious effect is the blurring of the recorded image caused by the shearing between the image and the recording film. The image is moving at a velocity $v_i' A_o$ whereas the recording film is moving at a velocity $v_r' = v_i' A_o + v_i' \varepsilon$. Therefore, in tracking over an aperture width w_x, the shearing between the image and the correct spot on the film will be

$$s_x = \frac{w_x\, v_i'\, \varepsilon}{v_r'}. \tag{10.6}$$

If the spot size of a point image falling on the film is already the desired resolution size Δx_4, then shearing should be kept to a fraction of the resolution size, say $\Delta x_4/4$, to prevent image blurring. Therefore, it is required that the fractional error of the velocity ratio be

$$\frac{\varepsilon}{A_o} < \frac{\Delta x_4}{4w_x} = \frac{A_o\ \rho_{Ra}}{4p\ w_x} \tag{10.7}$$

For example, for ρ_{Ra} = 25 m, $A_o \simeq 0.2$, and w_x = 1 mm, the fractional error must be maintained to be less than 0.7% (0.2% for ρ_{Ra} = 6.5 m). Thus, it is required to be able to adjust the ratio between the two film velocities to within 0.7% accuracy. Also, A_o must be measured to within 0.7% accuracy which may be difficult to do in practice. Since the fractional error is inversely proportional to the aperture width w_x, a decrease in w_x would ease the constraint on the velocity ratio.

If the spot size of a point image is somewhat smaller than the required resolution size, then a larger shearing, say Δx_4, is tolerable. The fractional error in velocity ratio then becomes

$$\frac{\varepsilon}{A_o} < \frac{A_o\ \rho_{Ra}}{p\ w_x} . \tag{10.8}$$

In fact, in Section 9, the velocity v_r was purposely offset to give incoherent averaging, and (9.2) gives a fractional velocity error $\Delta v_r/v_r$ similar to (10.8).

Consider now the effects of time-varying velocity errors (flutter) of the film motion. A low-frequency flutter leads to positional errors, whereas a high-frequency flutter leads to blurring. To control these problems, the maximum instantaneous *displacement* error should be less than a fraction, say 1/4, of a resolution element. Thus the positional error of the interferogram film should be less than $\rho_{Ra}/(4p)$ and of the recording film, less than $\rho_{Ra}\ A_o/(4p)$. For example, for ρ_{Ra} = 25 m, instantaneous positional errors should be less than 37 μm for the input film and less than 7μm for the output film.

From the displacement error specification, the maximum tolerable flutter can be determined. Flutter is usually defined in percent as 100 $\Delta v/v_o$ where Δv is the peak-to-peak volocity error and v_o is the constant velocity. For flutter frequency f, the film velocity is

$$v(f) = v_o + \Delta v(f) \cos 2\pi ft \tag{10.9}$$

so that the displacement of the film is

$$d = \int v(f)\, dt \tag{10.10}$$

and the maximum displacement error is

$$\Delta d = \int_{-1/4f}^{1/4f} \Delta v(f) \cos(2\pi f t)\, dt = \frac{\Delta v(f)}{\pi f}. \tag{10.11}$$

Therefore at the interferogram, a flutter of

$$\frac{\Delta v_i(f)}{v_i} \leq \frac{\pi f\, \rho_{Ra}}{4pv_i} \tag{10.12}$$

is required. Similarly, for the recording film, the flutter should be

$$\frac{\Delta v_r(f)}{v_r} \leq \frac{\pi f\, \rho_{Ra}\, A_o}{4pv_r} = \frac{\pi f\, \rho_{Ra}}{4pv_i}. \tag{10.13}$$

The maximum tolerable flutter is proportional to frequency f, and this constraint would therefore appear to be very restrictive for very small f. However, in going from high to low frequencies, the nature of its effect changes from blurring to scale-factor variation. Since a small change in scale-factor is more tolerable than blurring, low-frequency flutter need not be specified as tightly as high-frequency. As an example, consider v_r = 1.0 mm/s. For ρ_{Ra} = 25 m, flutter should be less than 1.2% at 0.5 Hz and less than 23% at 10 Hz. Neither of these values seem very difficult to obtain.

11. CORRECTION ERROR AND FOCUS CONSIDERATIONS

11.1 TOLERANCE CONDITIONS FOR ABERRATIONS

To assess the effect of various aberrations or errors on the output of the correlator, it is appropriate to compare the actual point-spread function (impulse response) to the ideal unaberrated point-spread function. Comparison can then be made on the basis of criteria such as resolution and integrated-side lobe ratio. However, the required analysis can be laborious at best. For present purposes, it will be found much simpler to consider phase-error criteria. In this method, the wavefronts that lead to the ideal and aberrated point-images are compared. The ideal wavefront is a spherical wave centred on the ideal point-image; the aberrated wavefront departs from this sphere in some manner.

It was shown by Rayleigh that, for spherical aberration, if the aberrated wavefront departs from the reference spherical wavefront by less than $\lambda/4$, (i.e., by less than $\pi/2$ radians of spatial phase) then the intensity at the centre of the point image is decreased by less than 20% and the width of the main peak is scarcely increased. Later, it was found that this rule could be applied to certain other types of aberrations. This result has become known as *Rayleigh's quarter-wavelength rule* [8].

A more general criterion follows from Maréchal's work [8]. A point image is considered to be acceptable if its maximum intensity is ≥ 0.8 of the maximum intensity of the ideal image (i.e., the Strehl ratio is ≥ 0.8). The Strehl ratio is a measure used in optics and is related to the integrated-side-lobe ratio. To satisfy this criterion, it is found that the root-mean-square departure of the wavefront from the reference sphere should be $\leq \lambda/14$. In the following, Rayleigh's $\lambda/4$ rule will be utilized as it is simpler to calculate.

11.2 RANGE SPREAD

Several of the functions of azimuth distance x_f in (3.1) or of the functions of azimuth frequency f_x in (4.1) are dependent upon range r_o. Thus, for each value of r_o, the terms in x_f or f_x must be handled differently. The range-dependent azimuth-focussing term in (3.1) or (4.1) is handled easily by use of tilted focal planes. However, for the range-curvature function, such as shown in (7.1), the variation with r_o was neglected over a certain spread of values of r_o. The acceptable range spread is calculated below.

In (7.3) it is desired to cancel the range-curvature term, thus leaving an ideal spherical wave to form an ideal image. Any error in the cancellation results in an aberration of the ideal azimuth wave. Therefore, by Rayleigh's $\lambda/4$ rule, it is required that

$$|r_o - r_{or}| < \frac{2c_a p^2 q}{\lambda^2 f_r f_x^2} \tag{11.1}$$

where r_{or} is a reference range used for the correction matched filter and r_o is the range of the actual signal. At $r_o = r_{or}$ there is perfect cancellation of range curvature. The spread of ranges, $r_o - r_{or}$, over which good imagery is obtained is limited then by the maximum value of $f_r f_x^2$.

If range curvature is to be fully corrected in one step, then the maximum value of f_x is $B_x/2$ plus the frequency offset caused by the antenna pointing-error. From (4.4) and Table 4.2 it is seen that

$$f_x\Big|_{max} = B_x/2 + f_{xpy}\Big|_{max} + f_{xye}\Big|_{max} = 56 \text{ c/mm}$$

at the latitude of Shoe Cove. From Table 4.1,

$$f_r\Big|_{max} = B_r/2 = 19.4 \text{ c/mm}.$$

The range spread is then $|r_o - r_{or}| \leq |\pm 5.7|$ km. For a full 100 km swath, the slant-range swath width is 38.4 km so that a minimum of 38.4/(2 x 5.7) = 3.4 different range-curvature correction functions are required. Since 4 subswaths are to be used, the range curvature will be reasonably well corrected over each subswath.

In Section 7.4, it was seen that range curvature usually will be corrected by treating the three factors of (7.24) separately. For the basic range-curvature factor, the first factor in (7.24), the maximum value of f_x is only $B_x/2$ = 13.0 c/mm. Then $|r_o - r_{or}| \leq 106$ km, so that the basic range-curvature correction need not be altered over the entire full swath. The second factor in (7.24) is compensated by a lens rotation that is independent of r_o so that its range spread is infinite. The third factor causes an image offset and need not be considered here.

11.3 TRADE-OFFS BETWEEN RANGE-CURVATURE CORRECTION AND RESOLUTION

In this section, the effect on resolution of not doing range-curvature correction or of doing only partial correction will be considered. The phase factors on the right-hand side of (7.24) will be used in the analysis. If uncorrected, the first two factors lead to what will be called here a blurring of the point response. In general, the peak of a point image is decreased and its sidelobes are increased. These terms should not be called defocussing since a defocussing aberration has the form f_x^2 or f_r^2 and can, in principle, be corrected by adjusting the focus of the system. The third factor leads merely to a shift in range of the output image and will not be considered further.

Application of Rayleigh's 1/4λ rule to (7.24) results in the limit

$$\frac{\pi \lambda_r^2 r_o}{4 c_a} \left[\frac{f_r}{q}\right] [(f_x/p)^2 - 2 f_x f_s / p^2] \Big|_{max} \leq \frac{\pi}{2}. \tag{11.2}$$

The maximum value of f_r/q is $B_r/(2q) = 1/(2\rho_{rs})$ where ρ_{rs} is the slant-range resolution. The maximum value of doppler frequency is

$$f_{dmax} = \frac{VL}{r_o \lambda_r} \tag{11.3}$$

where L is the synthetic-aperture length. Thus,

$$f_x/p \Big|_{max} = \frac{c_a L}{r_o \lambda_r}. \tag{11.4}$$

The substitution of (7.25) and (11.4) into (11.2) leads to

$$\left| \frac{c_a L^2}{4 r_o \rho_{rs}} - \frac{c_a x_s L}{r_o \rho_{rs}} \right| \leq 1 \tag{11.5}$$

where $x_s = x_{py} + x_{ye}$. Since

$$L = \frac{\lambda_r r_o}{2 c_a \rho_a}$$

where ρ_a is the azimuth resolution, the limit in terms of resolutions becomes

$$\left| \frac{\lambda_r^2 r_o}{16 c_a \rho_{rs} \rho_a^2} - \frac{\lambda_r x_s}{2 \rho_{rs} \rho_a} \right| \leq 1. \tag{11.6}$$

The first term expresses the limit of the basic range curvature and the second expresses the limit of the linear cross-coupling. In the absence of pointing error, $x_s = 0$ and (11.6) becomes

$$\rho_{rs} \rho_a^2 \geq \frac{\lambda_r^2 r_o}{16 c_a}, \tag{11.7}$$

a result which has been obtained by several other workers following different approaches.

At the latitude of Shoe Cove, the offset x_{ye} caused by equivalent yaw is 10.9 km for r_o = 841 km (see Table 3.4). If it is assumed that the long-term average of the pitch and yaw offset x_{pyav}, is zero, then the average offset $x_{sav} = x_{ye}$ = 10.9 km. The worst combination of pitch and yaw is seen from Table 3.4 to be 9.3 km, so that the worst value of x_s is 20.2 km. Equation (11.6) has been solved iteratively for ρ_a and ρ_{rs} for 3 values of x_s: its maximum, its average, and zero (no pointing error). The results are tabulated in Table 11.1 where ρ_{rs} has been converted to ground range using the approximation $\rho_{rg} \simeq 2.7\ \rho_{rs}$ (see Table 3.3). Since range and azimuth resolution can be traded one for the other, it is useful to present several combinations. First, the resolutions were chosen to be equal. Second, ρ_{rg} was set at its nominal value of 25 m, and finally ρ_a was set at its nominal value of 25 m.

A number of interesting observations may be made from Table 11.1. For the average antenna pointing-error, a resolution of 60 x 60 m is possible without doing *any* correction of range curvature or of linear cross-coupling. In the presence of pointing error, the selection in one dimension of the nominal design resolution results in the resolution of the other dimension being seriously degraded. The smallest possible value of x_s is 10.9 - 9.3 = 1.6 km so that zero pointing error never occurs. Consider, however, the case where

TABLE 11.1

Values of ρ_a and ρ_{rq} Calculated from (11.6) for Various Offsets x_s and No Range-Curvature Correction

CRITERION	x_s km	ρ_a m	ρ_{rg} m
1. ρ_{rg} and ρ_a chosen to be equal	20.2	80	80
	10.9	59	59
	0.0	19.1	19.1
2. ρ_{rg} set at 25 m	20.2	258	25
	10.9	140	25
	0.0	10.1	25
3. ρ_a set at 25 m	20.2	25	268
	10.9	25	150
	0.0	25	5.1

the linear cross-coupling aberration is cancelled by appropriately rotating the shift lens so that the second term of (11.6) vanishes. The resulting resolutions are then the same as those calculated from (11.7) and listed in Table 11.1 for x_s=0. It is in fact possible to get 19 x 19 m resolution by using only correction of the linear cross-coupling factor. Since the range resolution is limited to about 25 m by the radar system, the 19 x 19 m resolution could not actually ever be achieved. However, if ρ_{rg} were set at its minimum value of 25 m, ρ_a = 10.1 m is achieved. This resolution is not far from the best possible of 6 x 25 m.

The conclusion that may be drawn from Table 11.1 is that correction of the linear cross-coupling aberration (by rotating the shift lens) gives a good improvement in resolution. However, correction of the basic range-curvature aberration (by techniques such as the ones given in Section 7.3) does not improve resolution very much. Therefore the correction of the linear cross-coupling aberration should be a top priority whereas the addition of a corrector for the curvature aberration is not so important. It could be viewed as a final fine adjustment to obtain the ultimate resolution.

Since basic range curvature requires so little correction, the conjecture that the approximate methods described in Section 7.3 were adequate is in fact correct. It also becomes obvious that a single setting of the range-curvature corrector is adequate for all subswaths and all latitudes - once set up, it need never be altered.

The different combinations of resolution listed in Table 11.1 are obtained by placing the appropriate stops at the transform plane in both dimensions. These stops limit the aberration, but also limit the maximum resolution. The use of the full aperture in an attempt to obtain maximum resolution will instead degrade resolution because the aberrations will be increased.

11.4 LATITUDE SPREAD

(a) Changes in $c_a p^2$ with latitude

From (3.1), the azimuth focussing term of the interferogram is $\exp[-j2\pi c_a p^2 x_f/(\lambda_r r_o)]$, which has a focal length F_x given by (3.12). A change in the factor

$$c_a p^2 = \frac{V^2}{c_a v_f^2} = \frac{V^2}{(1 + h_s/r_e)v_f^2} \tag{11.8}$$

will cause a defocussing aberration in the wavefront. The velocity V and the altitude h_s vary with latitude. Ideally, the velocity v_f of the recording film should be varied so as to hold $c_a p^2$ constant. However, it appears that, at least initially, this control will not be incorporated into the recorder. Without this control, it will be necessary to refocus the correlator a number of times during one pass. This number is calculated below for the viewing area of Shoe Cove.

From Section 3.2, V varies from 7642 m/s at $\phi_o = 30.6°$ to 7631 m/s at $\phi_o = 73.8°$, a change of 0.1%. Figure 9 of [4] indicates that h_s varies from 793.0 km at $\phi_o = 30.6°$ to 796.5 km at $\phi_o = 73.8°$. The variation of V^2/c_a with latitude is summarized in Table 11.2. The change in altitude has much less effect than the change in velocity and could probably be neglected.

TABLE 11.2

Variation of V^2/c_a With Latitude

		$\frac{1}{1 + h_s/r_e}$	V^2	$\frac{V^2}{1 + h_s/r_e}$
$\phi_{lat}=29°$	($\phi_o = 30.6°$)	0.8893	5.840×10^7 m^2	6.567×10^7
$\phi_{lat}=66°$	($\phi_o = 73.8°$)	0.8889	5.823×10^7	6.551×10^7
	Difference	-4.3×10^{-4}	-1.680×10^5	-1.569×10^5
	% of Change	-0.05%	-0.29%	-0.24%

If the processor is properly focussed for a value of V^2/c_a, $(V^2/c_a)_1$, but the signal has the value $(V^2/c_a)_2$ then the phase error is

$$\phi_e = \frac{2\pi\ (x_f - x_o/p)^2}{\lambda_r\ r_o\ v_f^2}\ [(V^2/c_a)_1 - (V^2/c_a)_2]. \tag{11.9}$$

From Rayleigh's $\lambda/4$ rule it is required that $\phi_e \leq \pi/2$ for the maximum value of x_f^2. The maximum value of x_f^2 equals the sum of 1/2 the aperture width plus $(x_{py} + x_{ye})/p$. From Table 3.5, the aperture width, is 80.5 mm for ρ_{Ra} = 6.5 m and 20.7 mm for ρ_{Ra} = 25 m. It can be shown that for multiple looks, the phase error must obey the $\lambda/4$ rule over the full aperture containing all the looks. Thus, for SEASAT-A, the aperture width to be used in calculating ϕ_e for 25 m resolution with four looks is the same as for 6.5 m resolution with one look. For $x_{py} + x_{ye} = 0$, the maximum phase error is given in Table 11.3 for azimuth resolutions of 6.5 m and 25 m. It can be seen that by using three or more different focal settings for one pass, the imagery will be adequately focussed for 6.5 m resolution or, for four looks, 25 m resolution. For 25 m resolution single-look operation, no refocussing is necessary over one pass.

TABLE 11.3

Maximum Phase Error Over One Pass Arising from Latitude Dependent Changes in V^2/c_a for r_o = 850 km.

Resolution	$x_f\|_{max}$	$\phi_e\|_{max}$	$\phi_e\|_{max}/(\pi/2)$
ρ_{Ra} = 6.5m	40.2 mm	4.99 radians	3.2
ρ_{Ra} = 25 m, four looks	40.2 mm	4.99	3.2
ρ_{Ra} = 25 m, one look	10.3 mm	0.33	0.2

Note that $(x_{py} + x_{ye})/p$ can be much larger than the aperture size so that ϕ_e can become very large. Strict application of the $\lambda/4$ law would then indicate ten or more refocussings would be necessary over one pass. Fortunately, more detailed study reveals a useful property of the image degradation. First consider a defocussed image formed from a signal with no pitch and yaw. Then as the pitch and yaw increase, the same defocussed pattern shifts along x_4. Thus, at the centre of the original image, the intensity falls rapidly with increasing pitch and yaw whereas the offset image has approximately the same intensity distribution as the image obtained with no pitch and yaw. The offset will be no more than about one or two resolution cells. If this is tolerable, then Table 11.3 is applicable also for maximum pitch and yaw. Note that these offsets are applicable only to already defocussed images - perfectly focussed images will have no offset no matter how large the pitch and yaw.

Finally note that the number of refocussings per pass indicated in Table 11.3 is for the full viewing area of Shoe Cove (29° to 66° latitude), which extends approximately 4200 km and takes approximately 9.1 minutes to cover. There is some indication that most users will require no more than 300 or 400 km of imagery from one pass. In such cases, only one focussing will be needed for any resolution.

(b) Change in r_o with latitude

The range r_o varies with altitude and thus, with latitude. For the nominal boresight at 20° from the vertical, the change in r_o with latitude is given in Table 11.4. The change in range r_o over the Shoe Cove viewing area is approximately 3.8 km.

TABLE 11.4

Range r_o of Boresight Ray at 20°

Latitude	Altitude km	r_o km
29°	793.0	850.97
Shoe Cove	795.0	853.14
66°	796.5	854.76
$\Delta r_o\|_{max}$		3.8

If the boresight range changes from r_{o1} to r_{o2}, the range signal will be shifted on the recording film by a distance $(r_{o2}-r_{o1})/q$. The image will still be properly focussed when correlation is performed, but, this properly focussed image will have an apparent shift in ground-range at the output of the correlator. Suitable range calibration of the output image film must be done to correct for this drift in position with latitude.

To complicate matters further, a variable range delay, as discussed in Section 12, causes the position of the range signal on the recorder CRT to be shifted. The changes in delay are in steps of about 9.5 μs, which corresponds to changes in range of about 1.4 km. A change in delay has the effect of, for example, taking the signal for range r_{o1} and placing it at range r_{o2}. When this happens, the correlator may become defocussed. If a signal from range r_{o1} is shifted to a position r_{o2} and correlated as though it were from an object at r_{o2}, a phase error,

$$\phi_e = \frac{2\pi c_a p^2 (x_f - x_o/p)}{\lambda_r} \left[\frac{1}{r_{o1}} - \frac{1}{r_{o2}}\right]$$

$$\simeq \frac{2\pi c_a p^2 (x_f - x_o/p)}{\lambda_r r_o^2} (r_{o2} - r_{o1}),$$

arises. The $\lambda/4$ rule can then be applied to calculate the maximum range spread tolerable for good focussing. Some results are given in Table 11.5. Thus, for 25 m resolution, single-look processing, changes of one or two 1.4 km units of range delay will not necessitate a refocussing. However, for the other cases, a range-delay change of even one 1.4 km unit will necessitate a refocussing. Furthermore, note that discrete changes of 1.4 km will not always exactly correct for the drift in range caused by altitude change. Therefore the output range must be continuously calibrated, taking into account both the range drift caused by continuous altitude changes and the range offset caused by the discrete range-delay changes.

TABLE 11.5

Maximum Range Difference Permissible for Proper Focussing

Resolution	$x_f\|_{max}$	$r_{o2}-r_{o1}$
$\rho_{Ra} = 6.5$ m	40.2 mm	0.81 km
$\rho_{Ra} = 25$ m, 4 looks	40.2 mm	0.81 km
$\rho_{Ra} = 25$ m, 1 look	10.3 mm	12.4 km

11.5 DEPTH OF FOCUS

In terms of wavefront, a focussing error is equivalent to an error in estimating the radius of the spherical wavefront. Therefore the $\lambda/4$ rule may be applied to the defocussing aberration. The azimuth focal-length of the interferogram is F_x given by (3.12). Suppose the image plane is misfocussed so that it is located a distance $F_x + \delta F_x$ from the interferogram. The difference in the radii between the actual wave and the reference wave that would converge to the misfocussed plane is δF_x. The distance between the two spheres at a distance x_f from the centre of the aperture is approximately $\delta F_x (x_f/F_x)^2/2$. The Rayleigh $\lambda/4$ rule then shows that the azimuth depth of focus is

$$\delta F_x = \pm \frac{\lambda F_x^2}{2x_f^2} = \pm \frac{1}{8\lambda} \left[\frac{\lambda_r r_o}{p^2 c_a x_f}\right]^2 . \qquad (11.10)$$

Again, there is a dependence on the maximum value of x_f. For no pitch and yaw, $x_f|_{max}$ is 40.2 mm for 6.5 m resolution or for 25 m resolution with four looks. For 25 m resolution with one look, $x_f|_{max}$ is 10.3 mm. Pitch and yaw will shift a defocussed image by up to a few resolution elements but otherwise do not alter the defocussed image. Therefore, pitch and yaw will not be included in determining the maximum value of x_f.

Similarly, for the range dimension, the depth of focus is approximately

$$\delta F_r = \pm \frac{\lambda F_r^2}{2r_f^2} = \pm \frac{c^4}{32\, r_f^2 s^2 q^4 \lambda} . \tag{11.11}$$

The maximum value of r_f to be used in (11.11) is, from Table 3.5, 8.3 mm. At output plane P_4, the depth of focus, when $M_r = 1$, are

$$\delta F_{x4} = M_a^2 \, \delta F_x = A_o^2 \, \delta F_x \tag{11.12}$$

and

$$\delta F_{r4} = \delta F_r . \tag{11.13}$$

Values for depths of focus are given in Table 11.6. A range of r_o = 850 km, A_o = 0.207 (subswath 2), and λ = 0.633 μm were used in the calculations. It appears that focussing can be achieved over a fairly wide range, even at 6.5 m resolution. For 25 m resolution and one look, the depth of focus in azimuth is very large.

TABLE 11.6

Depth of Focus at Input and Output Image Planes

	At Input Image Plane	At Output Plane, P_4
δF_x, 25 m resolution, four looks or 6.5 m resolution	± 4.7 mm	±0.2 mm
δF_x, 25 m resolution, one look	±71.3 mm	±3.1 mm
δF_r	± 2.1 mm	±2.1 mm

12. ANNOTATION, REFERENCE INDICATORS, AND RELATED TOPICS

It is necessary for the users to have on the output film some reference indicators for both azimuth and range. It would also be useful to have an indication of the orientation of the image. Since at this writing many of the annotation and reference parameters have not been fixed, this discussion is only preliminary and subject to revision.

The interferogram will be annotated as illustrated in Figure 12.1. A continuous line will be drawn along both sides of the film about 1/2 inch from

the signal region. Timing pulses of 1 ms duration every 100 ms generate timing marks every 4.0 mm. Along the same line there is generated at one minute intervals a time code that gives the time in seconds, minutes, hours, days and 100 days. This standard 36 bit NASA time code uses 2 ms and 6 ms pulses, to indicate a "0" or "1", every 10 ms. These become the time code marks shown in Figure 12.1(c), where the spacing is 0.4 mm and the widths are 0.18 mm and 0.34 mm. The edges will not necessarily be sharp as shown and there may be difficulty in detecting the difference between a 0.18 mm mark and a 0.34 mm mark. Further experimental work is required.

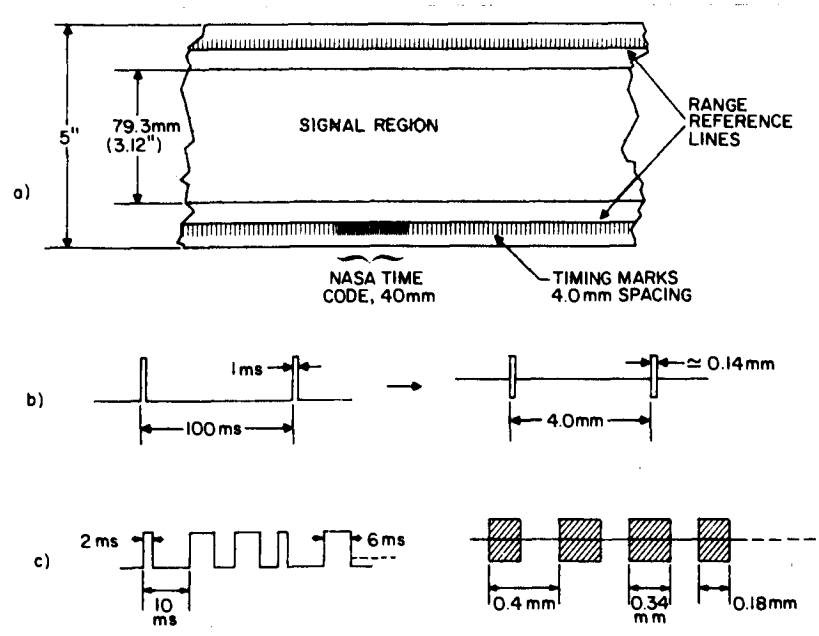

Figure 12.1. Annotation for interferogram film showing a) the interferogram b) the timing pulses and resulting timing marks, and c) time code pulses and resulting time code marks.

The annotation needs to be transferred from the interferogram to the image recording film. There will likely be a separate image film for each of the 4 subswaths. Therefore all 4 films need annotation. There is no intention to splice the film together to give a single 100 km map. This operation will be left to the user if he requires it.

For the azimuth reference marks, an optical detector needs to be placed near the interferogram to detect the timing marks and the time code. The detected signals could be relayed directly to the output film via a LED writer. However, it would be more useful to convert the time code to alphanumeric characters that are readable by the user. At JPL, time marks will be given every second, and time in numeric characters every 10 seconds of satellite flight time.

The range reference lines are more difficult to transfer. Perhaps, initially, the lines on the interferogram would not be used in range calibration. Nonetheless, there should be range reference marks (as at JPL) or a continuous range reference line placed on the image film.

Calibrating the range reference line then becomes the problem. For this purpose these will be generated on board the satellite a signal called the "retriggered chirp" which is added to the SAR signal. This linear FM signal is identical to the range linear FM signal. It is generated such that, upon processing in the correlator, a compressed range line appears on the output film. This line forms a very accurate range reference. There is a problem however. It is not presently known how to calibrate the reference line. In fact, it is not even known in which of the 4 subswaths the retriggered chirp will appear, or even if it will appear in any of the four subswaths. Therefore, it may be necessary to depend on the quality of the edge guiding of the various films, or to use some "ground truthing" to establish a range reference.

The azimuth and range references are the most important auxillary data that needs to be recorded. It would be useful, however, to have certain other data. These are discussed below.

a) Satellite Velocity

The satellite velocity, V, as a function of time (GMT) is available "prepass", i.e., before each satellite pass, via Telex from Goddard Space Flight Center. As discussed in Section 11.3, it would be beneficial to use this information to control the velocity v_f, of the recording film so that demagnification factor p could be maintained constant. However, it appears that, at least initially, this control will not be incorporated into the recorder. Therefore, it will be necessary during correlation to refocus, alter the magnification, and alter the film velocity ratio v_r/v_i. In order for these changes to be made correctly, the satellite velocity as a function of GMT must be known. This information could be obtained either from the original prepass data or from postpass data. The timing marks and time code marks on the interferogram would have to be read to determine the matching GMT.

b) Range-Delay Change

During the recording of the interferogram, a coherent trigger is used to trigger the sweep of the recorder's CRT. The coherent trigger is delayed from the PRF pulse by $n\tau/64$, where τ is the PRF period $1/f_p$. During a pass the integer n is changed as required so that the best part of the range antenna pattern is always recorded. Normally there will be only one or two changes per pass at Shoe Cove. When one of these changes occurs, the recorded signal is shifted in range relative to the interferogram film and the calibration of the range reference line must be changed. More important, because the azimuth focus is range dependent and the range has been shifted, the correlator must be refocussed. The correlator operator must therefore know when such changes in range delay occur. As with satellite velocity information, the range delay as a function of GMT is available prepass. Ideally this information should be annotated on to the interferogram film. However, initially it likely will not be. Therefore, the correlator operator must be given this information and he must search the timing marks on the interferogram to find the location of changes in range delay.

Another approach would be to use a constant-range-delay trigger. The advantages are that no refocussing is ever needed and the discrete jumps in range calibration are eliminated. However, a constant delay can result in

some loss of data. First, note that a range delay change of $\tau/64 = 1/(64 \times 1647) = 9.5$ μs corresponds to a slant-range shift of $3 \times 10^8 \times 9.5 \times 10^{-6}/2 = 1.4$ km. Therefore each half-subswath of film would lose about 1.4 km of imagery if the range-delay change were not utilized. Thus in each 19.2 km half-swath (see Figure 3.2) a loss of 7% of the imagery would occur. If the maximum number of changes were 2 and the constant delay were chosen to be the average of $n\tau/64$, then part of the time there would be no loss of imagery, and the rest of the time the maximum loss would be 7%. This loss seems tolerable in view of the advantages gained.

There are at least two ways to generate a constant-range-delay trigger. The PRF pulse could be used to trigger commercially available digital delay generators. Alternatively, the PRF pulse could be used and a constant delay generated by counting the 45 MHz sample clock also available during recording of the interferogram.

c) Attitude Data

Attitude data appear to be useful only for resolving doppler-centroid ambiguities, and are available only postpass. The Attitude-Orbit-Tracking tapes have been recommended as the best source of these data. These tapes must be processed on a computer such as the CRC Sigma-9 to extract the required attitude data as a function of GMT.

d) PRF

The PRF is of some use in determining the width of the frequency-plane azimuth-frequency window; however, it does not appear to be a critical parameter, so that no great effort should be expended to record it. The PRF is available prepass and since it remains constant for a given pass, it might best be recorded by simply hand printing it on the container of exposed film.

e) Vertical Velocity

Vertical velocity is available pre- and post-pass. However, as pointed out in Section 3, its overall effect is similar to that of pitch, and can be absorbed in the pitch and yaw terms of the various equations. Pitch and yaw are sensed as a composite effect during doppler-centroid estimation. It is suggested that values of vertical velocity need not be recorded.

f) Compass Heading or Track Orientation

In airborne SAR, usually the flight paths are straight and along only one compass heading. However, for a satellite, the azimuth direction has a varying compass heading because the ground track has a varying heading. Although it does not appear that JPL is going to do so, it would be very useful to certain users to indicate compass heading every 100 km or so. Compass heading or track orientation could be indicated by imaging an arrow-shaped light source, such as an LED, on to the recording film during correlation. A precision rotation mount would be adjusted to give the correct orientation and the light source flashed every 100 km or so. It would be necessary to compute the orientation from orbital data as a function of GMT. Prepass orbital data should be sufficient for this purpose.

13. GENERAL SUGGESTIONS FOR SYSTEM DESIGN

The general design philosophy should be to produce a good quality point-image with low distortion in range. Therefore, the design should involve end-to-end ray tracing, with considerable attention being paid to output quality and less attention being paid to the quality of intermediate planes. For example, it is not necessary to have a good quality Fourier transform provided the output image is of good quality.

In designing the JPL correlator, the designer at Perkin-Elmer starts with a suitable description of the interferogram and then performs all calculations and ray tracings from there through to the final image. Various optical elements are altered until the desired image quality is obtained.

M. Failes of CIR Ltd. is considering a variation of the Perkin-Elmer approach. He would like first to design the correlator while ignoring range curvature. When the end-to-end analysis indicates good quality images have been attained, he would then like to introduce range-curvature correction. The range-curvature corrector would also be designed using end-to-end analysis. Use of this procedure might mean that the shift lens may have to be altered, but the basic correlator design and construction can be commenced earlier. As a consequence the range-curvature corrector may become more difficult to design, but since it is composed of fewer elements than the remainder of the correlator, this added complexity may not be excessive.

It is not known to the author the exact form of description of the interferogram that was given to the designer of the JPL correlator. For the design of the DREO correlator, the mathematical description (3.1) - (3.3) and focal lengths (3.12) and (3.13) ought to be useful. It may also be useful to convert the interferogram into an equivalent lens as described in [9]. The problem may then be approached from a strictly lens design point of view. Such equivalent lenses typically have very small curvatures and very large refractive indices.

Although it may not be necessary to have high quality Fourier transforms, good quality may be fairly easy to achieve with little extra effort. Note that for f/8 or slower, good quality Fourier transforms can be obtained from almost any reasonable lens. Such f-numbers can be achieved for large apertures by using long focal lengths. Such extra length poses no great problem for the proposed DREO correlator. Wynne [10] has pointed out how simple doublets can be used to produce high-quality Fourier transforms. Using deviation of the wavefront from a reference sphere as the measure of quality, he reports that deviations less than $\lambda/10$ are produced.

It is required, of course, that the correlator telescopes be decoupled. It is strongly recommended that the range telescope have exactly unity magnification, preferably with $F_{s1} = F_{s2}$. Unless there is unity magnification, all calculations and adjustments become much more complicated. As well, as noted in Section 5.2, a variable azimuth-magnification (zoom feature) is required, which implies 3 or more lenses in the azimuth telescope.

The wavelength of the laser illumination is of some importance. A He-Ne laser that delivers 20 mw at 632.8 nm (red) is available at DREO. A krypton-ion laser is also available; it has 12 wavelengths to choose from.

The more useful ones are 647.1 nm (red) at 500 mw and 530.9 nm (green) at 200 mw. Recording films tend to be more sensitive to green light than to red. He-Ne lasers are in greater use and have a reputation for being more reliable than ion lasers. It has been suggested that the correlator be designed to operate in both the red and green portions of the spectrum, perhaps with a refocussing required when the wavelengths are switched. The ERIM correlator has this dual-wavelength capability. However, M. Failes points out that the design and implementation is made much more difficult if multi-wavelength operation is required. At present, the favored decision is to design the correlator for operation using red light so that either the He-Ne or krypton-ion laser may be used. The antireflection coatings on the lenses may be designed accordingly.

Some method of manipulating the film in the vertical direction must be devised since interferogram film contains 2 quarter-swaths that will be processed individually. Several options are available. If the optical flats in the liquid gate were approximately quarter-swath wide, the film could be shifted up or down in the liquid gate, or, the film could be turned over in going from one quarter-swath to the other. If the optical flats were as wide as the 5" film, then the entire liquid gate could be shifted up and down, or, as at JPL, a double mirror system could be used to offset the light from the film so that it runs along the optical axis of the telescopes. Some consideration should be given to making the film device sufficiently versatile so that not only can the quarter-swaths specified previously (see Figure 3.2) be centred in the aperture, but also any other quarter-swath can be processed. This facility would be especially useful for studying the boundary regions between the subswaths shown in Figure 3.2. For the proposed DREO correlator there is no overlap of image provided between subswaths, whereas at JPL some overlap is provided.

M. Failes has suggested the use of perchloroethylene as the index-matching fluid in the liquid gate. It apparently is less toxic than the commonly used xylene. It appears worthwhile to test this fluid.

Focussing will obviously be a considerable problem. Calculations can be made to determine the settings for the various components, but with such settings it is not likely that perfect focus will be obtained. Therefore, it will be necessary to do the fine focussing by eye. The focussing is, of course, best done with images of land. A good aid in focussing will be the retriggered chirp. Its line image will appear in one subswath and will provide an excellent reference for focussing in range. The final adjustment of the tilt angle of the output plane will also be critical. If velocity feedback is not used during the recording of the interferogram then refocussing during one pass may be necessary. In Section 11.3 it was estimated that, for 25 m resolution, 4 looks, and maximum pitch and yaw, approximately 3 focussing adjustments will be required during one pass. No refocussing will be required for 25 m resolution, 1 look, or for processing a partial pass. After each adjustment, the azimuth magnification A_o must be remeasured very accurately, and if it has changed even slightly, then the film velocity ratio v_r/v_i must also be altered accordingly.

There is some concern about the weighting of the spectrum arising during the recording of the interferogram. In range there is the direct effect of fall-off of MTF of the CRT, recording lens, and recording film. Since the

spectrum is offset in range frequency, the effect of MTF fall-off is to put an unsymmetrical weighting on the range spectrum, with the low frequencies having the least attenuation and the highest frequencies having the most. In separate analysis with A.W. Bridgewater of CRC it was shown that the image shape of a point object is about half-way between the sinc x_4 shape obtained for a rect spectrum and the smoothed shape obtained for a symmetrically tapered spectrum. It was concluded that no effort need be expended to correct for the MTF-induced weighting. In fact, this weighting may be just the one desired to give the best combination of resolution and integrated-sidelobe ratio. In azimuth, the weighting problem is more complicated. The non-zero width of each PRF line recorded on the interferogram leads to a weighting of the spectrum as illustrated in Figures 4.2 and 4.3. The azimuth spectrum shifts under this window because of pitch and yaw. Usually the resulting azimuth spectrum will be asymmetric but not monotonically decreasing with frequency, as with the range spectrum. Switching between spectral orders as discussed in Section 7.2 will ensure that the azimuth-frequency weighting does not become excessive.

A useful technique has been developed recently at Goodyear Aerospace wherein color film is used to improve the dynamic range of the output recording. As is well known, the output image can have a large dynamic range whereas the black and white film commonly used for recording the image has a relatively small dynamic range. Thus, information is lost. With appropriate use of color film, low light intensities are recorded normally at the color of the laser wavelength. However, if the light at some points is sufficiently intense, an additional color can be stimulated on the film. Thus intensity becomes color coded, thereby increasing the dynamic range.

14. SUMMARY

A system design for an optical correlator intended to produce imagery from interferograms recorded from the SEASAT-A SAR has been presented. It was decided to use the tilted-plane form of optical processing rather than the tilted-lens form. A mathematical description of the recorded interferograms is given as a basis for devising processing techniques, and relevant parameters of SEASAT-A and the interferograms are tabulated. The focussing properties of the interferogram are then described, and values tabulated. The two-dimensional Fourier transform of the interferogram is described mathematically. This description points the way to methods of range-curvature correction. The effects of the sampling in azimuth at the PRF are included in the description of the transform.

The basic tilted-plane optical correlator is described with emphasis on the SEASAT-A application. With normal processing, the tilt angle of the output image would be impractically large. Coincidentally it was found that, over the subswath widths to be processed, the slant-range-to-ground-range conversion is approximated closely by a simple magnification. The implementation of this magnification not only calibrates the output in the more desirable ground-range scale, but it considerably reduces the tilt angle to a practical value.

The hyperbolic form of the interferogram of a point object as recorded from the SEASAT-A SAR causes the azimuth image to lie on the opposite side of

the interferogram from the range image. It is necessary to shift one of these images so that it is closer to the other, and in particular so that both lie on the same side of the interferogram. The lens used for such shifting is described.

Antenna pointing-errors caused by pitch, yaw and earth rotation result in a shift in the envelope (but not the phase) of the SAR signal spectrum. These shifts cause the processing beam to be deviated at an angle to the optical axis of the correlator, and would normally be sufficient to require the use of impractically large diameter lenses. To overcome this problem a beam-steering mirror is used to incline the angle of incidence of the light illuminating the interferogram. The angle is chosen so that the spectrum is centred on the optical axis and the lenses can be of a more reasonable diameter. The output image is still located in its correct position, but a small distortion is introduced. If desired, this distortion can be corrected by a simple rotation of the output recording slit and film. Furthermore, it is shown how any one of the repeated azimuth spectra may be easily utilized to produce good images.

The effects of range-curvature is made worse by antenna pointing-errors. The range-curvature aberration can be separated into three components, each of which can be corrected separately. The first is the basic range-curvature aberration that would be the total aberration in the absence of antenna pointing-errors. For SEASAT-A this component is negligible for all but the highest azimuth-resolution (6.5 m). Two methods of correction are presented; one method simply involves a very small tilt of the shift lens. The second component, the linear cross-coupling component, gives rise to an image blurring that worsens as the antenna pointing-error increases. Although a small rotation of the shift lens is sufficient to correct for this component, the angle of rotation must be varied with antenna pointing-angle. The third component merely results in a shift of the output image. This shift varies with antenna pointing-angle and a slight distortion is introduced because of the range dependence of this shift. In many applications, such a shift is acceptable and may be neglected.

In order to centre the doppler spectrum on the optical axis, it is necessary first to locate the centre of this spectrum. Measurement of the doppler centroid is probably best done in a separate operation prior to correlation. Searching for a peak between two valleys, either visually or with photodetectors, appears to be as good a method of centroid estimation as any.

Multiple-look processing to reduce microwave speckle is relatively simple to implement on an optical processor. However, it seems more appropriate to obtain full azimuth resolution (6.5 m) with a single look rather than reduced resolution (25 m) with four looks.

Parameters of the output image-plane such as aperture size and spatial-frequency requirements are listed in Table 10.1. The film drive requirements turned out to be not as stringent as first feared. For example the ratio of output-to-input film-velocity need only be within 0.7% of the correct value for 25-m resolution and 1-mm image-plane slit. Even this restriction may be eased as the slit is made smaller.

In Section 11 the effects of not perfectly correcting for various aberrations are considered. Rayleigh's quarter-wavelength rule is established

as the basis of judging image quality. Most of the aberrations encountered depend on range, latitude or both. Since it is difficult to use a different correction for every value of range or latitude, the spreads of range over which a single correction yields an adequate image are calculated. For a worst-case antenna pointing-error, the range spread for range-curvature correction is found to be ±5.7 km. However, if range curvature is separated into its three components and the image-shift component is neglected, it is found that the other two components have a range spread wider than a full swath so that *no* adjustments need ever be done as range varies. It is then shown that resolution can be exchanged for range-curvature correction. It is found, for example, that for the average antenna pointing-error, a 60-m x 60-m resolution is possible without doing any correction. By correcting only the linear cross-coupling component, a resolution of 10.1 m in azimuth by 25 m in range can be achieved. It is found that the latitude spread is sufficiently large that only three changes in focus would be necessary over the entire Shoe Cove viewing region for the best (6.5 m) azimuth resolution. Unfortunately, any changes in the range delay of the SAR's electronics will generally require a refocussing unless appropriate shifts are built into the SAR recorder. Finally, the depth of focus of the correlator is calculated and found to be reasonably large - ±0.2 mm at the output plane for 6.5 m resolution and ±3.1 mm for 25 m resolution.

The annotation used on the interferogram to provide necessary orbit information is described. The suggested format of the output image film is briefly discussed. Comments on system design and miscellaneous items are given in Section 13. The principal recommendation is the obvious one that the lens design for the correlator be concluded by an end-to-end analysis.

15. ACKNOWLEDGEMENTS

Acknowledgements to several specific contributions were made in the text. However, in a report of this nature, which brings together a multitude of concepts, ideas, and techniques, it is impossible to adequately acknowledge every contribution. Instead, it must suffice to give general acknowledgement to various institutions and individuals. In particular, the author gratefully acknowledges the important contributions of staff at DREO and specifically Dr. N. Brousseau via extensive meetings, discussions and written communications. The contributions of M. Failes of C.I.R. Ltd. is similarly acknowledged. Two visits with T. Bicknell of J.P.L. provided an enormous amount of invaluable information and ideas. An early visit to ERIM provided excellent basic knowledge of optical correlators. The contributions of CRC staff and in particular those of G.E. Haslam and M.R. Vant are acknowledged with thanks. Finally, staff of the SURSAT office provided valuable contributions and contacts.

This work is supported by the Department of National Defence under Research and Development Branch Project 33D16.

16. REFERENCES

[1] Felstead, E.B. and G.E. Haslam, *Optical Recorder Design Considerations for the Canadian SEASAT-A Ground Station*, CRC Tech Note No. 695, November 1978.

[2] Felstead, E.B., *A Unified Formulation of Synthetic-Aperture Radar Theory*, submitted for publication.

[3] Kozma, A., E.N. Leith and N.G. Massey, *Tilted-Plane Optical Processor*, Appl. Opt. vol. 11, pp. 1766-1777, August 1972.

[4] *Mission Design for SEASAT-A*, JPL Document PD622-22, February 1977.

[5] Rayces, Juan L., *Nature and Correction of the SAR Range-Curvature Aberration*, Annual Meeting O.S.A., November 1973.

[6] Goodman, J.W., *Introduction to Fourier Optics*, McGraw-Hill, New York, 1968, p. 87.

[7] Zelenka, J.S., *Comparison of Continuous and Discrete Mixed-Integrator Processors*, J. Opt. Soc. Am., vol. 66, pp. 1295-1304, November 1976.

[8] Born, M. and E. Wolf, *Principles of Optics*, Third Edition, Pergamon Press, Oxford 1965, p. 468.

[9] Sweatt, W.C., *Describing Holographic Optical Elements as Lenses*, J. Opt. Soc. Am., vol. 67, pp. 803-808, June 1977.

[10] Wynne, C.G., *Simple Fourier Transform Lenses - I and II*, Optics Comm., vol. 12, pp. 266-274, November 1974.

FELSTEAD, E.B.
--System-design considerations
for an optical correlator...